OXFORD UNIVERSITY PRESS | Nucleic Acids Research

DNA polymerase gamma mutations that impair holoenzyme stability cause catalytic subunit depletion

Journal:	*Nucleic Acids Research*
Manuscript ID	NAR-04047-J-2020.R1
Manuscript Type:	1 Standard Manuscript
Key Words:	mitochondrial disease, DNA polymerase gamma, mitochondrial DNA, LONP1

DATA AVAILABILITY

Does the manuscript use or report the following? If so, please provide details in a Data Availability statement below and in the manuscript.	
New genome expression or sequencing data (ChIP-seq, RNA-seq…) - Must comply with ENCODE Guidelines. - All datasets must be validated via biological replicates. - Must deposit data in GEO or an equivalent publicly available depository and provide accession numbers, private tokens, reviewer login details and/or private URLs for Referees. - Excluding RNA-Seq, data must be viewable on the UCSC (eukaryotes) or other suitable genome browsers; must provide genome browser session links (even if GEO entries are publicly available).	**No**
Novel nucleic acid sequences - Must deposit in EMBL / GenBank / DDBJ. - Must provide sequence names and accession numbers.	**No**
Illumina-type sequencing data - Must submit data to BioProject/SRA, ArrayExpress or GEO. - Must provide link for reviewers (BioProject/SRA), login details (ArrayExpress) or accession numbers and private tokens (GEO).	**No**
Novel protein sequences - Must deposit UniProt using the interactive tool SPIN. - Must provide sequence names and accession number.	**No**
Novel molecular structures determined by X-ray crystallography, NMR and/or CryoEM/EM - Must deposit to a member site of the Worldwide Protein Data Bank (RCSB PDB, PDBe, PDBj) and provide the accession numbers. - If structures are unreleased (i.e. status HPUB), **MUST** upload: - the validation reports (.pdf) - molecular coordinates (.pdb or .mmcif). - one of the following: • X-ray data (.mtz, .cif) • NMR restraints and chemical shift files (.mr, .tbl or .str) • CryoEM map files (.map).	**No**
Novel molecular models based on SAXS, computational modeling, or other combinations of strategies that are generally not appropriate for deposition in the PDB - Must deposit coordinates and all underlying data in appropriate databases (including but not limited to the Small Angle Scattering Database and PDB-Dev). - Must report on validation of the structure against experimental data (if available) or report on statistical validation of the structure by model quality assessment programs. If applicable, these should be uploaded as a Data file.	**No**
Molecular behaviour studies derived from biological NMR spectroscopy data (not necessarily leading to new structures)	**No**

- Must deposit NMR spectral data, including assigned chemical shifts, coupling constants, relaxation parameters (T1, T2, and NOE values), dipolar couplings, in BMRB.	
Novel nucleic acids structure - Must deposit to NDB (via PDB if possible) and provide accession numbers.	**No**
Structures of nucleosides, nucleotides, other small molecules - Must deposit in the Cambridge Crystallographic Data Centre (CCDC) and provide the structure identifiers.	**No**
Mass spectrometry proteomics - Must deposit to ProteomeXchange consortium and provide Dataset Identifier and reviewer account details. If appropriate, data and corresponding details can also be deposited in the Panorama repository for targeted mass spec assays and workflows.	**No**
Microarray data - Must comply with the MIAME Guidelines - Must deposit the data to GEO or Array Express, and provide accession numbers and private tokens (GEO) or login details (ArrayExpress).	**No**
Quantitative PCR - Must comply with the MIQE Guidelines. - Details should be supplied in Materials and Methods section of manuscript.	**Yes**
Synthetic nucleic acid oligonucleotides including siRNAs or shRNAs - The manuscript should include controls to rule out off-target effects, such as use of multiple siRNA/shRNAs or inclusion of cDNA rescue data. - Manuscript should provide exact sequences, exact details of chemical modifications at any position, and source of reagent or precise methods for creation. These can be included in the main text or in Supplementary Material.	**Yes**
Flow Cytometry experiments - Must deposit in FlowRepository. - Must provide Repository ID and URL with secret code for Referees.	**No**
Software and source codes - Must deposit in GitHub and provide link to code in GitHub or upload source code as Data file.	**No**
Gel images, micrographs, graphs, and tables - Optionally, may deposit in a general-purpose repository such as Zenodo or Dryad. If applicable, provide access details.	**Yes**

Data availability statement. Please copy and paste data availability statement from manuscript text, including any accession numbers, login details, or reviewer tokens.
The data that support the findings of this work are available from the corresponding authors upon request

We thank the reviewers for their positive comments on our work and for their helpful suggestions. We have tried to address all the concerns raised to the best of our abilities.

Referee: 1

Comments for the Authors
The manuscript by the groups of Drs. Falkenberg and Viscomi demonstrate that the A467T recessive mutation of POLG results in a decreased binding for the processive subunit POLγB and that the apoenzyme (POLγA) is prone to be degraded by the LONP1 protease.
The authors use a very elegant approach with a plethora of tools (mouse model, biochemistry, cellular biology) to beautifully support their findings. The manuscript is well written, and the data support the main conclusions of the manuscript. The mouse model and cellular biology data differentiate this manuscript for a previous study "The Common A467T Mutation in the Human Mitochondrial DNA Polymerase (POLG) Compromises Catalytic Efficiency and Interaction with the Accessory Subunit" published by the Copeland group.
Accordingly, to this reviewer, there are two points that deserve attention in order to improve the manuscript. The hypothesis proposed by the groups of Drs. Falkenberg and Viscomi is directly related to the cellular concentrations of POLγA and POLγB. This reviewer assumes that both polypeptides are present in similar concentrations in mitochondria, however, this information is not present in the manuscript. The differences in dissociation constants between wild-type and the A467T mutant are only 3 to 5-fold different. Because of the small differences, it is important to know the concentrations of POLγB with respect to POLγA. For example, in a hypothetical case that POLγB would be 100 X more abundant than POLγA the conclusion that the free POLγA is degraded by LONP1 loses its strength.

To address the reviewer's comment, we have now quantified POLγA and POLγB in mouse tissues and HeLa cells. The POLγB dimer is more abundant than POLγA (5 to 10-fold), supporting the notion that POLγA is the limiting factor for complex formation. We would also like to point out that several lines of *in vivo* evidence support our conclusion that POLγA is a substrate for LONP1 and that complex formation with POLγB prevents POLγA degradation.

1) Depletion of LONP1 by siRNA leads to an increase in POLγA levels.
2) Depletion of POLγA by siRNA does not affect POLγB levels.
3) Depletion of POLγB by siRNA leads to a decrease of POLγA levels.
4) POLγA levels are increased in *Lonp1*$^{-/-}$ heart samples compared to control littermates.

We also have strong biochemical evidence, demonstrating that POLγA in free form is a substrate for LONP1 degradation, whereas the POLγ holoenzyme and POLγB are not. In addition, size-exclusion chromatography reveals a direct interaction between LONP1 and POLγA.

During our quantification of POLγB *in vivo*, we noted that the native protein migrates at a higher than predicted apparent molecular weight in extracts from mouse tissues and human cells. To follow up on this observation, we verified the specificity of the two commercial antibodies used by depleting POLγB in cell lines (using siRNA). The reason for the difference between the predicted and observed size of the protein is not known to us, but could indicate that the cleavage site for the leader peptide is different from what has previously been reported in the literature. Alternatively, POLγB may contain post-translational modifications that affect its migration in SDS-PAGE. The finding warrants future investigations and we have included our observations in Supplementary Figure 7.

A second point that is maybe convenient is the use of the crystallographic data by Whitney Yin´s group regarding the crystal structures of the holoenzyme in complex with dsDNA and in its absence. In the opinion of this reviewer, a figure showing the localization of residue A467 within the context of POLγB would help to understand how this mutation weakens the interaction. For instance, is residue POLγA-A467 in direct contact with POLγB? Could the mutation POLγA-A467T disrupt the folding of POLγA and in consequence alter its binding to POLγB and also decrease catalysis? Structural analysis may be useful to speculate about the direct consequences of the A467T mutation.

We have followed the reviewer's suggestion and have added a structural model of the mutation in Supplementary Figure 7.

This reviewer took the liberty to enumerate numerous minor comments, with the aim to improve the manuscript.

1.- Please add line numbers to facilitate the revision (word document)

Ok.

INTRODUCTION

1.- The POLG gene codes for the 140 kDa POLγA subunit that harbors DNA polymerase, 3'–5' exonuclease, and 5'–deoxyribose phosphate lyase activities (2)

Please add the reference
Genomics
. 1996 Sep 15;36(3):449-58. doi: 10.1006/geno.1996.0490.
Cloning and characterization of the human mitochondrial DNA polymerase, DNA polymerase gamma
P A Ropp 1, W C Copeland

Done

2.- "Interestingly, analysis of POLGA449T/A449T mouse tissues reveals a dramaitc depleation of mutant Polγ2" change to "Interestingly, analysis of POLGA449T/A449T mouse tissues reveals a dramatic depletion of mutant PolγA"

Done

3.- "by loss of interactions" please reword as the interaction is not abolished, but weaken.

The sentence has been reworded as suggested.

METHODS

4.- fragment of 769bp, which is cleaved in the A449T allele producing two fragments of 490bp + 279bp

please consider the following observation:

fragment of 769 bp, which is cleaved in the A449T allele producing two fragments of 490 bp + 279 bp

Done

Please consider adding a space between the number and "bp". Please revise the complete manuscript. The same applies for mM, nM, ng, etc

Done

5.- (final concentration: 20ng/µL) vs (final concentration: 20 ng/µL).

Done

6.- and supernatant was ethanol precipitated vs and the supernatant was ethanol precipitated.

Done

7.- The authors may want to present Material and Methods as a supplement.

We will be happy to move the Materials and Methods to the Supplementary material, but would leave this decision to the editor.

8.- 5× dye in assay buffer (50 mM Tris-HCl pH 7.8, 10 mM DTT, 50 mM MgCl2 and 5 mM ATP). Please revise how to write $MgCl_2$.
Why the authors use ATP in this buffer?

This is a standard buffer, which we use to analyze the stability of replication factors. For some replication factors (e.g. TWINKLE), ATP is required, but for others, like POLγ, ATP is not needed. ATP could therefore have been omitted from this specific experiment.

RESULTS

9.- "However, a significant reduction in treadmill", please consider using the percentage of reduction instead of the word significant.

The text has been changed as suggested.

10.- The same comment applies to this paragraph "significant reduction in spontaneous rearing movements"

The text has been changed as suggested.

11.- "Post-mortem hematoxylin and eosin staining at both ages did not show any gross abnormality in any tissue". Please add this data to the supplementary materials

These data have now been included as Supplementary Figure 4.

12.- Fig.2A. This reviewer assumes that the authors present WB analysis for 5 independent extractions. This should be clarified in the manuscript.

The reviewer is right. This has now been specified in the figure legend.

13.- Fig 2A PolγB is detected by WB analysis as a double band in brain tissues. Is this a degradation product? A posttranslational modification? Please indicate the presence of this double band

As discussed in our response to the general comment given by the reviewer (see above), we have noted that PolγB isolated from mouse tissues and human cells migrates at a molecular weight slightly higher than predicted. This observation could indicate the existence of a posttranslational modification in vivo and the double band observed in brain could potentially support this notion. However, for the time being, we believe that it is more likely that the additional band is due to cross-reactivity with an undefined, brain-specific protein (as suggested in the figure legend).

14.- It would be possible to measure the concentrations of PolγB and PolγA in different tissues?

This kind of analysis has been performed in plant mitochondria and possibly in animal mitochondria. If this is the case the authors may want to consider adding this information to their manuscript

Please revise figure 5 of the following article published in The Plant Journal

Single organelle function and organization as estimated from Arabidopsis mitochondrial proteomics
Philippe Fuchs Nils Rugen Chris Carrie Marlene Elsässer Iris Finkemeier Jonas Giese Tatjana M. Hildebrandt Kristina Kühn Veronica G. Maurino Cristina Ruberti

A sophisticated quantitative assay as the one described in the suggested paper is beyond the scope of the present study. However, to address the reviewer's concerns, we have quantified the ratio between POLγA and POLγB in mouse tissues and HeLa cells (please see above). The results demonstrate that POLγB is present at higher levels than POLγA.

15.- Fig 3B. This reviewer assumes that each of the 4 bands present in SKM and liver tissues is a biological replica for the long-range PCR. If this is the case, this reviewer observed no difference between PolgA449T/A449T and WT littermates for skeletal muscle and liver tissues. However, the authors present data that indicates that the mt copy number is reduced in skeletal muscle but not in liver (Fig 3A). This reviewer is confused about those observations and would appreciate it if the authors shed some light to reconcile the data or to explain it.

We are grateful for the question and have now specified this point in the figure legend. Figure 3B represents 4 biological replicas for each tissue. The data presented in Figure 3A were obtained by real time, quantitative PCR. The long-range PCR is done as an endpoint reaction and is thus not quantitative.

16.- The data present in Figs 3C to 3J nicely shows an increase in replication intermediaries in t PolgA449T/A449T that the authors associate with a defect in mitochondrial DNA replication.

We thank the reviewer for his/her positive comment.

17.- This reviewer is confused about Fig 4C. The gels show no difference between full-length replication products by PolgA449T/A449T and WT mice and show a clear appearance of replication intermediates in the PolgA449T/A449T mouse. It is unclear why there are no differences in the full-length replication products, the obvious phenomena should be a decrease in the full-length replication product. How a DNA polymerase that is less effective or that is targeted for its degradation incorporates in total more labeled dATPs? This is counterintuitive for this reviewer. Do the cells in the PolgA449T/A449T mouse compensate by having more mitochondria? This reviewer apologizes in advance for this question.

There are two answers to this questions. First, with regard to the levels of full-length mtDNA, In wt cells, about 95% of all replication events are terminated at the end of the D-loop, forming 7S DNA. In PolgA449T/A449T mice, we observe a dramatic drop in 7S DNA, which is typically associated with impaired mtDNA replication. In other words, to compensate for impaired replication, all replication initation events are used for full-length mtDNA replication. If the molecular defect caused by A449T had been stronger, we would expect to also see

mtDNA depletion. However, given the relatively mild phenotype, compensatory mechanisms, such as the observed drop in 7S DNA formation, can compensate for the mutant phenotype.

Second, due to the impaired activity the mutant A449T polymerase, we also obtain more replication intermediates, proably caused by stalling. These types of abberant replication products are normally degraded and therefore not observed. The exact mechanism is not known, but mitophagy has been invoked. In our experiments, we use isolated mitochondria and many of the cellular pathways used to degrade abberant mtDNA are therefore not active. Abberant replication products therefore remain intact and when radioactive dNTPs are added, they get labelled, by POLgA-A449T, which can initiate DNA synthesis from any free 3'-end.

18.- Fig. 5 In the opinion of this reviewer a figure showing the structural localization of residue POLgA-A449 would be illustrative.

We have followed the reviewer's suggestion and have now added this figure as Supplementary Figure 8.

19.- "less than POLγA WT (Figure 5A and Supplementary Figure 6A) and remained substantially lower than the WT also after the addition" please refer to the decrease in Kd (in fold decrease)

The text has been modified as suggested.

20.. Fig 5C and Fig 5H show contradictory data. In Fig 5C POLγAWT and mutant POLγAA449T are active and inactive (only at a high dNTPs concentration a band is observed in POLγAA449T). However, in a long circular ssDNA template, the amount of product between POLγAWT and mutant POLγAA449T is very similar. The difference is that in Fig 5H the authors add TWINKLE and mtSSB. The authors may want to refer to several studies by the groups of Drs. Smita Patel and Charles Richardson regarding the stimulatory effects of T7 DNA helicase in T7 DNA polymerase. These experiments in Fig 5C may indicate that in the "context" of a replisome the catalytic activity due to the POLγAA449T mutation is not severely compromised. The authors seem to have a different conclusion from the data present in Fig. 5H. Please quantify the data in Figs 5H and 5I to address this concern.

This is a misunderstanding, due to poor labeling of our figures. Fig 5C and fig 5H should not be compared. In fig 5C, we perform the experiment in the absence of POLγB and under these conditions, the A449T mutant is virtually inert. However, when we add PolγB to the reaction (Fig 5D) the function is rescued to near wt levels. Since POLγB is present also in fig 5H (required for replication on double-stranded DNA), the data in fig 5H should be compared to fig 5D. To avoid this confusion, we should have labelled the figures in a better way! We have now made changes to the panels in fig 5, to indicate when POLγB is present.

The quantification of the blots in Figures 5H and 5I are presented in Supplementary Figure panels 7D and 7E. Supplementary Figure 7D is a dot blot representation of aliquots from the assays in Figures 5H and 5I. The dots are subsequently quantified individually and data are presented in Supplementary Figure 7E. Our analysis confirmed that both the mouse A449T and human A467T mutants are slower than the WT enzymes. Notably, the effect is most evident with the human replisome.

21.- Figs 6 and 7. Very clear and well-executed experiments. As the authors state "Collectively, these results support that LONP1 specifically targets POLγA both in cells and in vivo".

Thank you again for the very positive comment.

DISCUSSION

The discussion is very short and contrasts with the detailed results sections. The authors may want to write a combined Result/Discussion section if this is possible or in its defect rewrite the discussion.

We have revised the discussion, trying to make it more comprehensive.

Referee: 2

Comments for the Authors
This paper explores a new mouse model of POLG disease generated by Crispr KI of the human equivalent of the common pathogenic POLG A467T variant. While a severe phenotype was not observed in the homozygous KI mouse, the authors noted reduced exercise tolerance and rearing movements. Analysis of the KI tissues and MEFs showed reduced POLgA protein levels coincident with reduced mtDNA content and 7S DNA. In vitro analysis of the recombinant PolgA-A449T demonstrated reduced polymerase activity, reduced stability and impaired interaction with the PolgB accessory subunit, all consistent with the literature values for the human A467T PolgA. Further analysis revealed that the accessory subunit helps to stabilize the catalytic subunit even though it displays some unfolding. Investigation of the reduced PolgA A449T protein revealed that the protein is being digested by the mitochondrial Lon protease. This was substantiated by siRNA knockdown of the Lon protease in Hela cells and with heart tissue from Lonp-/- mice. In vitro analysis also demonstrated that the PolgA, but not PolgB was a substrate for the Lonp and that the presence of the PolgB accessory subunit prevent degradation of PolgA by Lonp.

Overall, this is an interesting paper that potentially sheds light on the pathology of several of the POLG mutations.

Comments
1. Perhaps this is beyond the scope of this investigation, but since this is the first occurrence of a POLgA disease mouse model, I would like to see the affect during aging, out to 2 years of life. What is the life expectancy of this mouse compared to WT mice? Are there any classical age-related phenotypes?

We monitored the lifespan of our mouse model up to two years of age, but no obvious, age-related phenotype was detected. We added a sentence noting this point to the Result section.

2. Fig 2A. Please describe what the five lanes are for each tissue. Are these from different mice? Also, Why is there a doublet for POLγB in both the WT and A449T mouse in the brain samples but not any of the other tissues?

Figure 2A represents biological replicas for each tissue (this is now specified in the legend). As for the additional band in the brain, we interpret it as a tissue-specific band, as specified in the legend. Please also see our response to reviewer 1, point 13.

3. It is unclear what recombinant PolγA and PolγB proteins, mouse or human, were evaluated in vitro. The reference, Ref 24, is for the human proteins, while the nomenclature is for the mouse residue. Please clarify and include in the

manuscript which proteins, human or mouse, were analyzed in vitro. Also, there are no methods regarding the expression and purification of the mouse proteins.

Which PolγB is being used in the human A467T POLγA vs mouse A449T PolγA comparison? Is the PolγB only from mouse, or only from human, or both? Please clarify.

In the new version of the manuscript, we now better specify the proteins uses in each experiment. We have also included a method section describint the expression and purification of the mouse proteins.

4. Why does both POLgB and POLgA knockdown result in an increase of LONP1? (Fig 6F, comparing si-control to siPOLgB and siPOLgA in the LONP1 lanes). What is the explanation for this? The paper really needs an explanation here. Perhaps the reduction in POLG and subsequent reduction in mtDNA causes more free TFAM which requires more LONP1, but that seems like a stretch.

LONP1 has many other targets in vivo and is required for multiple mitochondrial functions, including gene expression. The exact reason for the increase in LONP1 levels is therefore difficult to define, since the increase most likely is a part of a more general stress response. This role of LONP1 in mitochondrial function has been carefully studied in previous reports (Zurita Rendón O, Shoubridge EA. LONP1 is required for maturation of a subset of mitochondrial proteins, and its loss elicits an integrated stress response. Mol Cell Biol. 2018 Sep 28;38(20):e00412-17. doi: 10.1128/MCB.00412-17).

5. Need to discern why Lon protease is digesting POLG. Is it because it (the mutant) is unstable and not folded correctly, or is it because of the absence of the accessory subunit? The evidence in this paper suggest that the digestion of the wt POLgA is only due to be isolated (not protected) from the PolgB subunit, but that could be a consequence of the PolgA being partially unfolded.

As demonstrated here, both WT and mutant POLγA can be degraded by LONP1. The POLγA protein appears to be intrinsically unstable and POLGγB is required for its stabilization and protection from LONP1. Mutant POLγA binds less efficiently to POLγB and is thus more easily degraded by the protease. Even if this is the primary effect of A467T, we cannot rule out that the mutation also further destabilizes the structure of POLγA and thus contribute to LONP1-dependent degradation in this manner. In support of this notion, the thermofluor stability assay revealed no major differences in the profile between $mPOL\gamma A^{WT}$ and $mPOL\gamma A^{A449T}$ from 37 °C upwards, but the fluorescence signal of $POL\gamma A^{A449T}$ was already higher than the WT at 25 °C, indicating that the mutant protein was already partially unfolded even at temperatures below 37 °C (Figure 6A and 6B). However, *in vitro*, wt and A467T POLγA are degraded with similar efficiency (Figure 7B).

6. I would like to see more introduction-background of the Lon protease in regards to the historical finding that free TFAM is a substrate for Lon.

As suggested by the Reviewer, we have now added some background information on LONP1.

Referee: 3

Comments for the Authors
1. Thank you very much for sending me this manuscript from Silva-Pinheiro et al. to review. This is a thorough investigation of a common pathogenic mutation in mtDNA polymerase gammaA, both in vivo using a similar mutation in mice and in vitro. The major observation is that mice carrying the POLGA mutation show a decrease in steady state levels of the protein. The authors then show convincingly that the decrease is due to increased susceptibility to degradation

by LonP1, very likely because the mutation reduces the affinity between POLGA and POLGB subunits resulting in more free POLGA. The experiments have been performed well and I generally can argue against little in this nice work. However, there are a couple of issues I would like to see addressed before publication.

Perhaps the most confusing aspect of the work is that there only a mild depletion of mtDNA in the mice in all tissues analysed, yet they show physiological phenotypes. Could the authors please comment on this? In the end, we would expect any phenotype to be due to modulation of oxidative phosphorylation due to an effect on mtDNA gene expression. If there is no difference in the level of intact mtDNA and it is presumably the final readout of any POLG mutation, how can there be any alteration in phenotype? Presumably, the authors have measured steady state OXPHOS protein levels and biochemical analyses. Is any defect noted? The response to liver degeneration is an interesting expt but as the depletion seemed greatest in SKM how would they respond to muscle degeneration? Don't worry, I'm not suggesting you do that expt for publication!

We agree with the reviewer that the mice results are surprising, given the severity of the human diseases associated with POLG mutations. However, we want to point out that the mouse model does indeed display a mild reduction of mtDNA levels in skeletal muscle, which fits with the slightly reduced treadmill performance. From the biochemical point of view, we only found a mild, non-significant reduction of complex I in skeletal muscle, which may be in keeping with the very mild reduction in motor performance. However, we want to stress that in the MEFs the phenotype becomes obvious after inducing depletion with EtBr. We agree with the reviewer that carrying out further experiments would be interesting, but it is beyond the scope of the current work. However, we have expanded the discussion and now address this issue.

2. Could the authors please compare what they find in the mouse model with what is seen in patients cell lines with this common recessive mutation? This is important, as we need to judge whether this mouse would be a useful model for POLG mutations.

We agree with the reviewer that this experiment would be important. However, even after interrogating several clinical research centers worldwide, we have been unable to obtain homozygous A467T fibroblasts. There are however many other examples of patient derived fibroblasts with various POLG mutations that present decreased mitochondrial DNA repopulation rates following induced depletion by EtBr. As reported here, we found that A449T mutant MEFs did not repopulate mtDNA after EtBr depletion, whereas wt MEFs recovered to pretreatment levels within 3 days (Fig 3G). We have included a section about this in the discussion along with a relevant reference describing problems with mtDNA repopulation in in POLG mutant fibroblasts (J.D. Stewart et al, Biochim Biophys Acta 2011, 1812:321-5). Additionally, we would like to stress that the in vitro data presented here, revealed similar defects in the mouse and human proteins, supporting the idea that the molecular consequences of the mutations in the mouse protein are similar to, but less severe than those observed for the human protein.

3. It is always possible to come up with additional expts and I'm not suggesting the authors need to perform this expt prior to publication but it would be interesting to see whether it is possible to rescue the ethidium bromide depletion by overexpressing polGB, as this may lead to an increased level of POLGB in mitochondria raising it above the KD necessary for the mutant polyGA to bind.

This is an excellent suggestion, which will warrant future investigations to determine the possibility of overexpressing PolyB as a treatment option.

4. Fig 6B – this is surprising, as the thermal melt expts show that whilst the addition of POLGB leads to a substantial increase in stability of the POLGA due to complex formation, there is no difference in the profile between the wild type and the mutant polGA either alone or in complex. Is this not surprising?

Our interpretation of this experiment is that the addition of POLγB stabilizes both wt and mutant POLγA. Since the experiments were performed in the presence of saturating levels of POLγB, we did not see a distinct difference between the two proteins. Please also see our response to Reviewer 2, point 5.

5. Finally, I found much of the discussion rather repetitive of the results section. Perhaps a bit of editing is in order?

We reshaped the discussion as requested also by the other reviewers.

Wild-type

Polg A449T/A449T

PolγA

PolγB

Stable
Polγ complex

Unstable
Polγ complex

LonP1

PolγA
degraded

PolγA
degraded

PolγA protected

PolγA protected

mtDNA

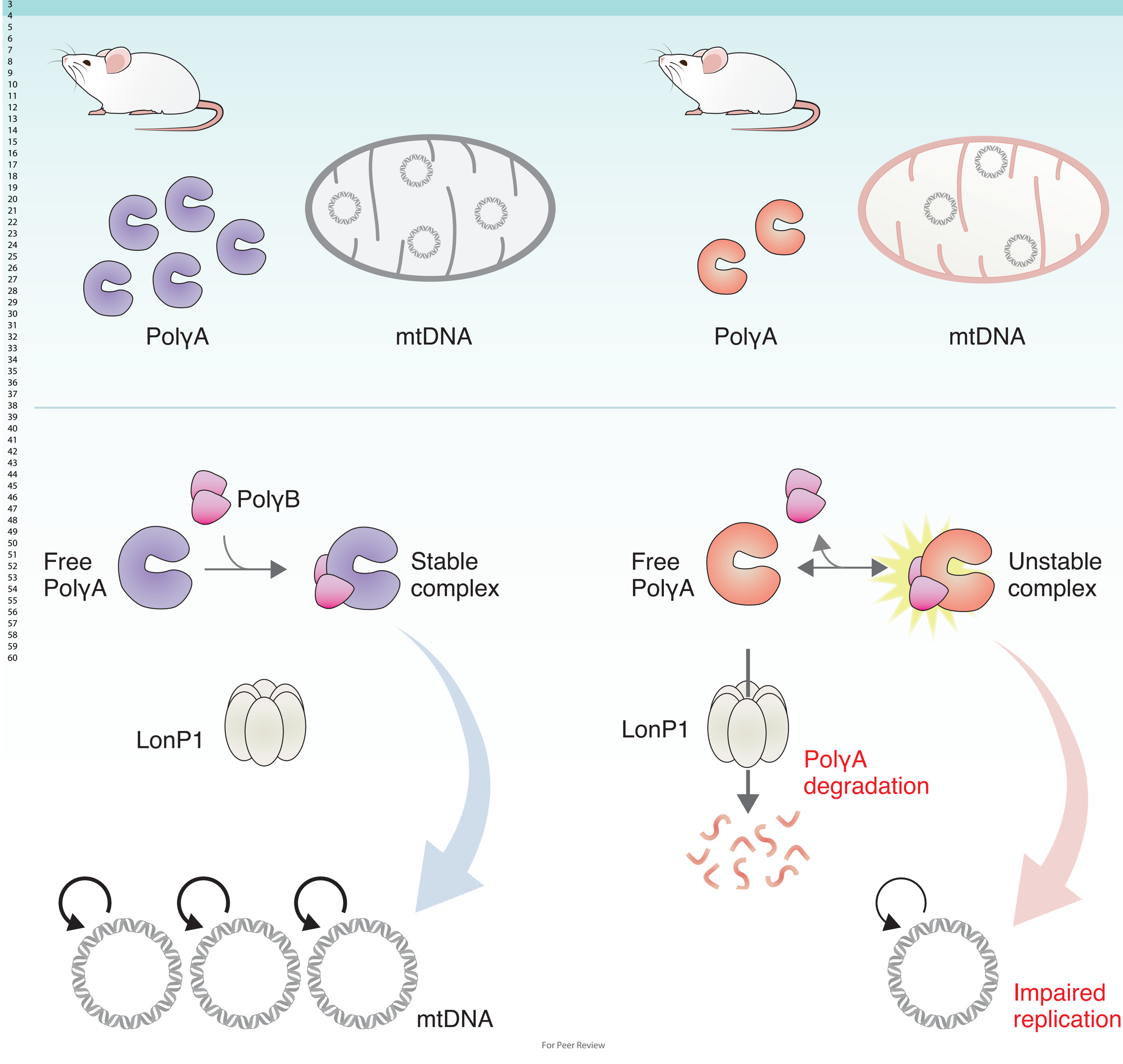
Wild-type
Polg A449T/A449T
PolγA
mtDNA
PolγA
mtDNA
PolγB
Free PolγA
Stable complex
LonP1
mtDNA
Free PolγA
Unstable complex
LonP1
PolγA degradation
Impaired replication

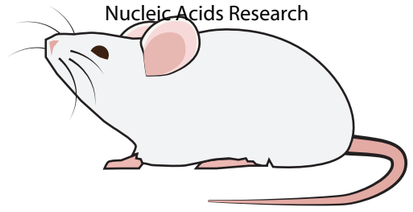

Wild-type

PolγA

PolγB

Polγ complex

LonP1

mtDNA

Polg A449T/A449T

Unstable complex

PolγA degradation

Impaired replication

mtDNA levels

DNA polymerase gamma mutations that impair holoenzyme stability cause catalytic subunit depletion.

Pedro Silva-Pinheiro[1,#], Carlos Pardo-Hernández[2,#], Aurelio Reyes[1], Lisa Tilokani[1], Anup Mishra[2], Raffaele Cerutti[3], Shuaifeng Li[4], Dieu Hien Ho[5], Sebastian Valenzuela[2], Anil Sukru Dogan[6], Bradley Peter[2], Patricio Fernandez-Silva[7], Aleksandra Trifunovic[5], Julien Prudent[1], Michal Minczuk[1], Laurence Bindoff[8], Bertil Macao[2], Massimo Zeviani[3,9], Maria Falkenberg[2,#,*] and Carlo Viscomi[10,#,*]

[1] MRC/University of Cambridge Mitochondrial Biology Unit, Hills Road, CB2 0XY, Cambridge, UK

[2] Department of Medical Biochemistry and Cell Biology, University of Gothenburg, Medicinaregatan 9A P.O. Box 440, SE405 30 Gothenburg, Sweden

[3] Department of Neurosciences, University of Padova, via Giustiniani, 2 - 35128 Padova, Italy

[4] Center for Cancer Biology, life science of Institution, Zhejiang University, Hangzhou 310058, China

[5] Cologne Excellence Cluster on Cellular Stress Responses in Aging-Associated Diseases (CECAD) and Center for Molecular Medicine (CMMC), University of Cologne, Joseph-Stelzmann-Str. 26, 50931 Cologne

[6] Department of Molecular Biology and Genetics, Center for Life Sciences and Technologies, Bogazici University, 34342, Istanbul, Turkey

[7] Biochemistry and Molecular and Cell Biology Dept., University of Zaragoza, C/ Pedro Cerbuna s/n 50.009-Zaragoza, and Biocomputation and Complex Systems Physics Institute (BIFI), C/ Mariano Esquillor, 50.018-Zaragoza (Spain)

[8]Department of Clinical Medicine, University of Bergen, Norway; Neuro-SysMed, Department of Neurology, Haukeland University Hospital, Jonas Lies vei 65, 5021 Bergen, Norway

[9] Venetian Institute of Molecular Medicine, via Orus 2 - 35128 Padova, Italy

[10] Department of Biomedical Sciences, University of Padova, via Ugo Bassi 58/B - 35131 Padova, Italy

#These authors equally contributed to the work

* Correspondence to:
Carlo Viscomi, PhD
Department of Biomedical Sciences
Via Ugo Bassi 58/B
University of Padova
Padova, Italy
Email: carlo.viscomi@unipd.it
Tel.: +39049 8276458

OR
Maria Falkenberg

1 Department of Medical Biochemistry and Cell Biology

2 University of Gothenburg

3 P.O. Box 440

4 SE405 30 Gothenburg, Sweden

5 Tel: +46 (0) 31 786444

6

7

Abstract

Mutations in *POLG*, encoding POLγA, the catalytic subunit of the mitochondrial DNA polymerase, cause a spectrum of disorders characterized by mtDNA instability. However, the molecular pathogenesis of *POLG*-related diseases is poorly understood and efficient treatments are missing. Here, we generate the *POLG*$^{A449T/A449T}$ mouse model, which reproduces the A467T change, the most common human recessive mutation of *POLG*. We show that the mouse A449T mutation impairs DNA binding and mtDNA synthesis activities of POLγ, leading to a stalling phenotype. Most importantly, the A449T mutation also strongly impairs interactions with POLγB, the accessory subunit of the POLγ holoenzyme. This allows the free POLγA to become a substrate for LONP1 protease degradation, leading to dramatically reduced levels of POLγA in A449T mouse tissues. Therefore, in addition to its role as a processivity factor, POLγB acts to stabilize POLγA and to prevent LONP1-dependent degradation. Notably, we validated this mechanism for other disease-associated mutations affecting the interaction between the two POLγ subunits. We suggest that targeting POLγA turnover can be exploited as a target for the development of future therapies.

Introduction

DNA polymerase γ (POLγ) is the main protein responsible for mitochondrial DNA (mtDNA) replication and mutations in its gene (*POLG*) are the most frequent cause of mitochondrial disease related to a single nuclear gene. POLγ consists of a heterotrimer with one catalytic POLγA subunit and two POLγB accessory subunits (1). The *POLG* gene codes for the 140 kDa POLγA subunit that harbors DNA polymerase, 3′–5′ exonuclease, and 5′-deoxyribose phosphate lyase activities (2,3), whereas *POLG2* encodes the 55 kDa POLγB, which stabilizes the interactions with template-DNA, thereby increasing processivity (4). POLγ is the only DNA polymerase required for mtDNA replication in mammalian mitochondria and, at the replication fork, it works in concert with the TWINKLE DNA helicase (5). The mitochondrial single-stranded DNA-binding protein (mtSSB) stimulates mtDNA synthesis by increasing the helicase activity of TWINKLE and the DNA synthesis activity of POLγ (6).

The A467T is the most frequent POLγA mutation in Scandinavian and Northern European Countries, together with another change, the W748S change, which seems to be part of the Finnish disease heritage (7-10). The intermediate region, where the two deleterious mutations are located, is defined as the "linker" region between the proofreading and the polymerase domain and seems to play a role in the binding to the accessory subunit POLγB. The mechanistic explanation of how these two mutations affect the activity of this important enzyme and lead to disease is not fully understood, but

in vitro, the A467T mutation reduces POLγA affinity for the POLγB accessory subunit and impairs the catalytic activity of POLγ (11). In addition to the A467T and W748S, over 300 mutations have been described in *POLG* (Human DNA Polymerase Gamma Mutation Database: https://tools.niehs.nih.gov/polg/). However, four mutations alone (A467T, W748S, G848S and the T251I–P587L allelic pair) account for ~50% of all mutations identified in patients with *POLG*-related diseases, with ~75% of patients carrying at least one of these mutant alleles (12). *POLG* mutations may lead to mtDNA instability, causing either multiple deletions or depletion (13). However, there is no obvious genotype–phenotype correlation, the same mutation can often lead to mtDNA deletions, mtDNA depletion or both. A prototypical example is the homozygous mutation A467T mutation, which has been associated with a range of phenotypes, from severe conditions as Alpers-Huttenlocher syndrome (AHS) to milder ones as myoclonic epilepsy myopathy sensory ataxia (MEMSA), comprising spinocerebellar ataxia with epilepsy (SCAE), frequently associated with sensory ataxia neuropathy with dysarthria and ophthalmoplegia (SANDO) (14). In addition, the age of onset and the progression of POLG-related disease in patients with the same *POLG* mutations is astonishingly variable and can span several decades. For instance, the onset of disease spans >70 years in compound heterozygous patients carrying the T251I–P587L mutations on one allele (15) and the G848S mutation on the other, and it spans at least four decades of life in homozygous A467T patients (16,17).

Maintaining mitochondrial protein homeostasis (proteostasis) is essential for most mitochondrial processes, including those involved in mtDNA maintenance. Mitochondrial proteostasis is ensured by proteases, which are involved in the regulation of the protein steady-state levels and degrade misfolded and/or unincorporated peptides. A particularly relevant role is carried out by LONP1, a AAA^+ protease of the mitochondrial matrix (18). LONP1 has three functional domains: a substrate recognition N-terminal domain, an ATP-binding and hydrolyzing AAA^+ ATPase domain, and a C-terminal protease domain. The LONP1 protein forms a hexameric cylindrical structure which recognizes its substrates and carries out protein unfolding and proteolysis in an ATP-dependent manner. In addition, LONP1 influences mtDNA levels by degrading the mitochondrial transcriptional factor A (TFAM) (19-21), a key factor in regulation of mitochondrial transcription initiation and packaging of mtDNA into nucleoprotein structures (nucleoids) (22). Notably, LONP1 mutations have been associated with mitochondrial disease (23).

We here establish a disease model, which reproduces the human A467T change in the mouse (*POLG*$^{A449T/A449T}$). *In vitro*, the mouse mutation, A449T, impacts polymerase activity in a way similar to what has been previously described for human A467T (11). Interestingly, analysis of *POLG*$^{A449T/A449T}$ mouse tissues reveals a dramatic depletion of mutant POLγA. We find that this depletion is explained by weakened interactions with POLγB. When POLγA is not bound to POLγB, it is susceptible to degradation by LONP1. Our results demonstrate a

protective role for POLγB and reveal a novel pathogenic mechanism for *POLG*-related diseases, which in turn may open new avenues for the development of future therapies.

Materials and Methods

Generation of *Polg*$^{A449T/A449T}$ mice

Polg$^{A449T/A449T}$ mice were generated by a double-nickase CRISPR/Cas9 D10A-mediated gene editing of mouse *Polg* gene in exon 7 (c.1345G>A / p.A449T). For a detailed representation see (Supplementary Figure 1A). The selected sgRNAs (Table 1) were cloned into plasmid pSpCas9(BB)-PX330 (Addgene #42230), using the *BbsI* site. The resulting constructs were used as a template to amplify by PCR the gRNA (spacer + scaffold) preceded by a T3 promoter to allow subsequent *in vitro* transcription. The *in vitro* transcription was carried using the MEGAscript T3 Transcription Kit (Life Technologies). The same kit was used to produce Cas9 D10A mRNA using as template the plasmid pCAG-T3-hCasD10A-pA (Addgene #51638). The 140 bp ssDNA homology direct repair (HDR) donor (Table 1) was acquired from IDT. Cas9 D10A mRNA, gRNAs and HDR donor were microinjected into fertilized FVB/NJ one-cell embryos (Core Facility for Conditional Mutagenesis, Milan). Genotyping of *Polg*$^{A449T/A449T}$ mice was performed by PCR (primers Polg_A449T_Fw + Polg_A449T_Rv, Table 1), followed by a restriction digestion with *PvuII*. WT allele produces a fragment of 769 bp, which is cleaved in the A449T allele producing two fragments of 490 bp + 279 bp (Supplementary Figure 1B). The PCR is carried using GoTaq DNA polymerase (Promega, UK) and

the following PCR conditions: 95 °C for 30 s, 63.7 °C for 30 s, and 72 °C for 1 min, 35 cycles.

Table 1. Oligonucleotides list.

Name	**Sequence (5′ - 3′)**	**Use**
sgRNA-Fw	GATGCCTGTCAGTTGCTCTC	*Polg*$^{A449T/KO}$ generation
sgRNA-Rv	GCGACTTCTTCATCTCCCGC	
140 bp ssDNA HDR donor	AGGCACAGAACACATATGAGGAGCTACAGCGGGAGATGAA GAAGTCGCTGATGGATCTGACTAATGATGCCTGTCAGCTG CTCTCAGGAGAGAGGTAGTCAGGTTCTGGGCAGGCTGGGT CAATGCAGGGTACAGGCAGG	
Polg_A449T_Fw	GTTGTCCCTGTCTTCCTCCA	Genotyping
Polg_A449T_Rv	AAGCTTCCCACCTTCCTGAT	
Polg_KO_Fw1	CTTCGTCGATCGACCTCGAATAAC	
Polg_KO_Fw2	GGATGGGCAGGAACAGTTAG	
Polg_KO_Rv	CTGCCATTCACCTTACCC	
Lonp1_KO_Fw	AGGTGACTGTGGAGAGATTCC	
Lonp1_KO_Rv	CTTCACTAGTGTCACAGACCT	
qPCR_mCoI_Fw	TGCTAGCCGCAGGCATTACT	qPCR and rt-qPCR
qPCR_mCoI_Rv	CGGGATCAAAGAAAGTTGTGTTT	
qPCR_RnaseP_Fw	GCCTACACTGGAGTCGTGCTACT	
qPCR_RnaseP_Rv	CTGACCACACGAGCTGGTAGAA	

qPCR_mNd4_Fw	TCGCCTACTCCTCAGTTAGCCA	
qPCR_mNd4_Rv	GATGTGAGGCCATGTGCGATT	
qPCR_Gapdh_Fw	CACCATCTTCCAGGAGCGAG	
qPCR_Gapdh_Rv	CCTTCTCCATGGTGGTGAAGAC	
LongR_mtDNA_Fw	GAGGTGATGTTTTTGGTAAACAGGCGGGGT	Long-range PCR
LongR_mtDNA_Fw	GGTTCGTTTGTTCAACGATTAAAGTCCTACGTG	
7S_probe_Fw	ATCAATGGTTCAGGTCATAAAATAATCATCAAC	Southern Blot
7S_probe_Rv	GCCTTAGGTGATTGGGTTTTGC	

Animal work

All animal experiments were carried out in accordance with the UK Animals (Scientific Procedures) Act 1986 (PPL: P6C20975A) and EU Directive 2010/63/EU. The mice were kept on FVB/NJ background, and wild-type littermates were used as controls. The animals were maintained in a temperature- and humidity-controlled animal care facility with a 12-hour (h) light/12-h dark cycle and free access to water and food, and they were monitored weekly to examine body condition, weight, and general health. The mice were sacrificed by cervical dislocation at 3, 12 and 24 months of age for subsequent analysis.

Lonp1 gene targeting (*Lonp1*$^{+/tm1a(EUCOMM)Hmgu/Ieg}$, project number HEPD0936_3_B11) was carried out as part of the The European Conditional Mouse Mutagenesis Program (EUCOMM), on the C57BL/6NTac

genetic background. We generated the heart and skeletal muscle specific *Lonp1* knockout mice by mating *Lonp1*$^{fl/fl}$ animals with transgenic mice expressing cre recombinase under the control of muscle creatine kinase promoter (*Ckmm-cre*) (19), after removal of a gene-trap DNA cassette. Experiments were performed on 12-week-old mice. The genotyping primers used are on Table 1 (Lonp1_KO_Fw + Lonp1_KO_Rv).

All experiments on *Lonp1*$^{fl/fl}$*; Ckmm-Cre* animals were approved and permitted by the Animal Ethics Committee of North-Rhein Westphalia (Landesamt für Natur, Umwelt und Verbraucherschutz Nordrhein-Westfalen; LANUV) following the German and European Union regulations.

Treadmill

A standard treadmill apparatus (Panlab) was used to measure motor endurance according to the number of falls in the motivational air puff during a gradually accelerating program with speed initially at 6.5 m/min and increasing by 0.5 m/min every 3 min. The test was terminated by exhaustion, defined as >10 air puffs activations/min.

Comprehensive laboratory animal monitoring system (CLAMS)

Mice were individually placed in the CLAMS™ system of metabolic cages and monitored over a 48-h period. Data were collected every 10 minutes (min). The parameters analyzed were: ambulatory and rear movements, VO_2 (volume of oxygen consumed, ml/kg/h), VCO_2 (volume of

carbon dioxide produced, ml/kg/h), RER (respiratory exchange ratio) and heat (kcal/h).

Pharmacological treatments

In VPA-treated mice, VPA (Sigma) was administrated by daily oral gavage (300 mg/kg in water) or added to a standard diet at 1.5% (1.5 g-VPA/ 1 kg-Food) and administered for 60 days, starting at 8 weeks of age.

In CCl_4 experiments, mice received a single IP injection of CCl_4 (1 mL/kg body weight diluted 1/10 in olive oil (Sigma). Mice were sacrificed after 2 or 4 days. For histology analysis of necrotic areas (see below), Hematoxylin and Eosin (H&E) staining was performed in livers samples. The quantification of necrotic areas was done with ImageJ by dividing the necrotic areas around the central veins by total area of the section. Five different regions of the slide were analyzed and average value obtained.

DNA and RNA extraction

Genomic DNA was extracted by resuspending samples in lysis buffer (0.5% sodium dodecyl sulfate (SDS); 0.1M NaCl; 50 mM Tris-HCl, pH=8; 2.5 mM EDTA). Samples were incubated overnight at 55 °C after adding Proteinase K (final concentration: 20 ng/µL). Next, samples were purified with 1 volume chloroform + 0.6 M potassium acetate and the supernatant was ethanol precipitated. Final DNA was eluted in water.

Total RNA was extracted from the indicated tissues using the TRIzol Reagent (Thermofisher) following the manufacture protocol.

Real-time quantitative PCR

For mtDNA relative quantification, SYBR Green real-time qPCR was performed using primers specific to a mouse mtDNA region in the COI gene. Primers specific to RNaseP, a single copy gene taken as a nuclear gene reference. All primers are listed in Table 1. Approximately 25 ng of DNA was used per reaction.

For the quantification of mRNA levels, cDNA was retrotranscribed from total RNA extracted using the Omniscript RT kit (Qiagen). For mitochondrial transcripts *CoI* and *Nd4*, specific primers (Table 1) were used as described above with SYBR Green chemistry. Expression was calculated using the ΔΔCt analysis using *Gapdh* as reference.

Specific Gene Expression TaqMan assays (Invitrogen) were used for *Polg* and *Polg2*. Expression was calculated using the ΔΔCt analysis using *B2m* as reference.

Long-range PCR

MtDNA was amplified from 50 ng of total DNA with the primers (LongR_mtDNA_Fw and LongR_mtDNA_Rv, Table 1) using PrimeSTAR GXL DNA polymerase (TAKARA, Japan) and following PCR conditions: 98 °C for 10 s, 68 °C for 13 min, 35 cycles.

Cell cultures

Polg$^{A449T/A449T}$ and control mouse embryo fibroblasts (MEFs) were prepared from individual E12.5 embryos and were cultured in complete Dulbecco's Modified Eagle Medium (DMEM) (4.5 g/L glucose 2 mM glutamine, 110 mg/ml sodium pyruvate), supplemented with 10% fetal bovine serum (FBS) and 5% penicillin/streptomycin. MEFs were seeded in six-well plates at 20% confluence. Cells were incubated with or without 100ng/mL EtBr for 5 days and DNA samples were collected every 24h. At day 5, cells new medium without EtBr was added and cells were allowed to recover for an additional 8 days. Again, DNA samples were collected every 24h. MtDNA quantification was performed as described above.

HeLa cells were grown at 37 °C, 5% CO2 in DMEM (4.5 g/L glucose, 2 mM glutamine, 110 mg/ml sodium pyruvate) supplemented with 10% FBS and 5% penicillin/streptomycin. For siRNA transfections, 0.3 x 10^6 HeLa cells were reverse transfected with 5 nM of siRNA using Lipofectamine RNAiMAX. siRNAs used in the study are: (i) *LONP1* (5´-GGUGCUGUUCAUCUGCACGtt-3´), (ii) *POLG2* (5´-CGGUGCCUUGGAACACUAUtt-3´), (iii) *POLG* (5´- CCCAUUGGACAUCCAGAUGtt-3´). After three days, cells were harvested, washed with PBS and used for Western Blotting as described above.

Immunofluorescence analysis and confocal imaging

Immunofluorescence was performed as previously described (24). Briefly, cells seeded in 24-well plate were fixed in 5% paraformaldehyde (PFA) in PBS at 37 °C for 15 min and incubated with

50 mM ammonium chloride in PBS for 10 min at room temperature (RT). After three washes in PBS, cells were permeabilized using 0.1% Triton X- 100 in PBS for 10 min, washed 3 times with PBS, and then blocked in 10% FBS in PBS for 20 min at RT. Cells were then incubated with indicated primary antibodies for 2 hours in 5% FBS/PBS, washed in 5 % FBS in PBS and incubated with secondary Alexa Fluor conjugated antibodies in 5% FBS/PBS for 1 hour at RT. We used the following antibodies: TOM20 (1:1000) was from Abcam (ab232589), DNA (1:1500) was from Millipore (CBL186), Goat Anti-rabbit Alexa Fluor 594 (1:1000) was from Invitrogen (A-11012), Donkey anti-mouse Alexa Fluor 488 (1:1000) was from Invitrogen (A-21202). EdU incorporation was detected using Invitrogen Click-iT EdU AlexaFluor 647 (Invitrogen, C10340) labelling kit according to manufacturer's instructions. Coverslips were mounted onto sides using Dako fluorescence mounting medium (Dako). Images were then acquired as 7 stacks of 0.2 µm each, using a 100X objective lense (NA1.4) on a Nikon Eclipse TiE inverted microscope using an Andor Dragonfly 500 confocal spinning disk system, equipped with a Zyla 4.2 PLUS sCMOS camera, exciting with 488 nm, 594 nm or 633 nm lasers, and coupled with Fusion software (Andor). For quantification of EdU or mtDNA number, max projection images were processed once with the "smooth" function in Fiji and nucleus was removed. Images were then manually thresholded, 'smoothed' and number of particles were obtained using the "Analyze particles" plugin in Fiji with a minimum area of 0.1 μm^2. The representative images in figure 3 were processed once with the "smooth" function in Fiji.

Biochemical analysis of MRC complexes

Liver and muscle samples stored in liquid nitrogen were homogenized in 10mM of potassium phosphate buffer (pH=7.4), and the spectrophotometric activity of respiratory chain complexes I, II, III and IV, as well as citrate synthase, was measured as described (25).

BNGE and in-gel activity

For blue native gel electrophoresis (BNGE) analysis, skeletal muscle and liver mitochondria were isolated as previously described (26). Samples were resuspended in 1.5 M aminocaproic acid, 50 mM Bis-Tris/HCl (pH 7) and 4 mg of dodecyl maltoside/mg of protein, and incubated for 5 min on ice before centrifuging at 20,000 × g at 4 °C. 5% Coomassie G250 was added to the supernatant. 100 µg was separated by 4%–12% gradient BNGE and further subjected to a Complex I in-gel activity (IGA), as previously described (27). To allow for cI activity to appear, gels were incubated between 1.5 and 24 h in cI-IGA reaction buffer.

Histological analysis

Mouse tissues for Hematoxylin and Eosin (H&E) analysis, were fixed in 10% neutral buffered formalin (NBF) for a few days at room temperature and then included in paraffin wax. Sections of 4 µm were

used for analysis. H&E staining was performed by the standard methods.

For COX/SDH histochemical analysis, skeletal muscle (gastrocnemius) samples were frozen in isopentane pre-cooled in liquid nitrogen. Sections of 8 µm were stained for COX and SDH activity as described (28).

Southern Blot

Three micrograms of total DNA isolated from each tissue were restricted using the restriction enzyme *BlpI* according to manufacturer's instructions (New England Biolabs). Products were separated on 0.8% agarose gels (Invitrogen Ultrapure) and dry-blotted overnight onto nylon membrane (GE Magnaprobe). Membranes were hybridized with radiolabeled probes overnight at 65 °C in 0.25 M phosphate buffer (pH 7.6) and 7% SDS, then washed for 3 × 20 min in 1 × SSC and 0.1% SDS and imaged using a phosphorimager (GE Healthcare) and scanned using an Amersham Typhoon 5 scanner. For primer sequences used for producing probes, see Table 1.

In Organello Replication

Labeling of mtDNA in isolated organelles was performed as previously described (29).

Briefly, isolated liver was minced and homogenized in 4 ml/g of tissue in Sucrose-Tris-EDTA (STE)-buffer [320 mM sucrose, 10 mM Tris-

HCl (pH 7.4), 1 mM EDTA and 1 mg/mL essentially fatty acid-free bovine serum albumin (BSA)] using a manual tight-fitting teflon pestle. Resulting mitochondria were washed once in STE-buffer, pelleted and equilibrated in incubation buffer [10 mM Tris-HCl (pH 8.0), sucrose and glucose 20 mM each, 65 mM D -sorbitol, 100 mM KCl, 10 mM K_2HPO_4 , 50 µM EDTA, 1 mg/mL BSA, 1 mM ADP, $MgCl_2$, glutamate and malate 5 mM each]. In organello labeling was performed for 5; 15; 30; 60 and 90 minutes, at 37 °C with rotation, using 1 mg/mL mitochondria in incubation buffer supplemented with dCTP, dGTP and dTTP (50 µM each) and [α-^{32}P]-dATP (Hartmann, 3000 Ci/mmol) at 6.6 nM. At the end, DNA was extracted by solubilizing mitochondria with 1 % sodium N -lauroylsarcosinate, followed by 100 µg/mL Proteinase K on ice for 30 min and phenol-chloroform extraction. Gel electrophoresis, southern blotting and hybridization were carried as described above.

2D-AGE

For two-dimensional gels, DNA was extracted from fresh liver-isolated mitochondria purified by sucrose gradient followed by phenol-chloroform extraction. Five micrograms of the resulting mtDNA were restricted digested with *BclI* according to manufacturer's instructions (New England Biolabs). For first dimension, products were separated on 0.4% agarose gels (Invitrogen Ultrapure) without ethidium bromide. Then each lane was excised and rotated 90° anticlockwise for second dimension electrophoresis by casting around

the gel slices 1% agarose with 500 ng/mL ethidium bromide. After electrophoresis, southern blotting and hybridization were carried as described above.

Western Blot and Antibodies

Mouse tissues were homogenized in RIPA buffer [150 mM sodium chloride, 1.0% NP-40, 0.5% sodium deoxycholate, 0.1% SDS (sodium dodecyl sulfate), 50 mM Tris, pH 8.0] in the presence of protease inhibitors (cOmplete™ Protease Inhibitor Cocktail, Sigma). Protein concentration was determined by the Lowry method. Aliquots, 30 µg each, were run through a 12% SDS-PAGE and electroblotted onto a polyvinylidene fluoride (PVDF) membrane, which was then immunodecorated with different primary antibodies: anti-POLγA (1:500) was from Santa Cruz Biotechnology (sc-5931), anti-POLγB (1:1000) was from LSBio (LS-C334882), anti-GAPDH (1:3000) was from Abcam (ab53098), anti-LONP1 (1:1000) was from Proteintech (15440-1-AP), anti-HSC70 (1:1000) was from Santa Cruz Biotechnology (sc-7298). Secondary antibodies were from Promega (catalog nos. W4011 [rabbit], W4021 [mouse] and V8051 [goat]). HeLa cells were lysed in lysis buffer (0.125 M Tris HCl, pH. 6.8., 4% SDS and 500 mM NaCl). Whole cell lysates were quantified and 50 µg were resolved in 4-20% SDS-PAGE and transferred onto nitrocellulose membranes (GE healthcare). The membranes were then incubated with the primary antibodies: anti-POLγA (1:1000) was from Abcam (ab128899), anti-POLγB (1:500) was home-made polyclonal from Agrisera, anti-LONP1 (1:1000)

was from Abcam (cat ab103809) and anti-β-actin (1:10000) was from Abcam (ab6276).

Quantification of POLγB and POLγA in mouse tissues was performed with enriched mitochondria fractions. Mouse tissues were homogenized in Buffer A [320 mM sucrose, 1 mM EDTA, 10 mM Tris-HCl, pH 7.4] followed by a centrifugation at 800 x g for 5 minutes. The supernantant was further centrifuged at 12000 x g for 2 minutes and the resulting mitochondria-enriched pellet was lysed with RIPA buffer and treated as descrived above. Each well was loaded with 10 µg of mitochondria-enriched protein extracts. Absolut quantification was performed using a standard curve with known protein concentrations of purified recombinant POLγA and POLγB. Ratio between POLγB (calculated as a dimer) and POLγA was calculated by dividing POLγB amount by 2 to obtain the amount of POLγB dimer. The final value was obtained by dividing the amount of POLγB dimer by the amount of POLγA. Ratio of (POLγB dimer)/ POLγA for HeLa cells was obtained with a similar method by using whole cell lysates as descrived above. During the course of our experiments, we noted that native POLγB migrates with an apparent molecular weight slightly higher than expected from previous predictions. The results were the same with two different antibodies (LSBio (LS-C334882 and Agrisera) and the specific recognition of the protein was verified by siRNA-depedent depletion of POLγB in HeLa cells.

Production of LONP1, TFAM, POLγA and POLγB, expression and purification

LONP1 (Wild-type and LONP1 ^{S855A}) gene lacking the mitochondrial targeting sequence (aa 1-67) was cloned into a pNic28-BSA4 vector with a cleavable 6xHisTag in the N-terminus. Rosetta™(DE3) pLysS competent cells (Novagen) were transformed with the plasmid and grown in Terrific Broth media with 50 mg/l Ampicillin and 34 mg/l Chloramphenicol at 37 °C until OD_{600} = 3. Protein expression was induced with 1 mM IPTG at 16 °C for 4 h.

Cells were harvested by centrifugation, frozen in liquid nitrogen, thawed and lysed at 4 °C in lysis buffer (25 mM Tris-HCl pH 8.0, 0.8 M NaCl and 10 mM β-mercaptoethanol). The suspension was homogenized using an Ultra-Turrax T3 homogenizer (IKA) and centrifuged at 20000 x g for 45 min in a JA-25.50 rotor (Beckman Coulter). The supernatant was loaded onto His-Select Nickel Affinity Gel (Sigma-Aldrich) equilibrated with buffer A (25 mM Tris-HCl, pH 8.0, 0.4 M NaCl, 10% glycerol and 10 mM β-mercaptoethanol). The protein was eluted with buffer A containing 250 mM imidazole. Removal of the 6xHisTag was achieved by overnight-dialysis in presence of ≈ 0.5 mg TEV in buffer A. An additional Nickel purification step was performed to get rid of uncut His tagged protein and TEV. The protein was subsequently purified over a 5 ml HiTrap Heparin HP column (GE Healthcare) and a 1 ml HiTrap Q HP column (GE Healthcare), both equilibrated in buffer B (25 mM Tris-HCl pH 8.0, 10% glycerol and 1 mM DTT) containing 0.2 M NaCl, followed by elution driven by a linear gradient (50 and 10

ml respectively) of buffer B containing 1.2 M NaCl (0.2-1.2 M NaCl). Protein purity was checked on a precast 4-20% gradient SDS-PAGE gel (BioRad, 567-8094) and pure fractions were aliquoted and stored at -80 °C. TFAM was expressed in bacteria and purified as previously described (20).

Human and mouse POLγA versions (lacking the mitochondrial targeting sequence aa 1-25) and human and mouse POLγB (lacking the mitochondrial targeting sequence aa 1-24 and aa 1-16 respective) were expressed in Sf9 cells and purified as described previously (30), with the following modifications. For POLγA, an additional step of purification with 1 ml HiTrap SP HP column was added after the HiTrap Q HP column purification. The column was equilibrated with buffer B containing 0.1 M NaCl and eluted with a linear gradient (10 ml) of buffer B containing 1.2 M NaCl (0.1-1.2 M NaCl). For POLγB, an additional step of purification with a 1 ml HiTrap Talon column (GE Healthcare) was used in between HiTrap Heparin HP (GE Healthcare) and HiTrap SP HP (GE Healthcare). This column was equilibrated with buffer C (25 mM Hepes pH 6.8, 10% glycerol, 0.4 M NaCl, 1 mM β-mercaptoethanol) containing 5 mM imidazole and elution driven by a linear gradient (10 ml) of buffer C containing 150 mM imidazole (5 mM-150 mM imidazole).

For the generation of mutant versions of POLγA, QuikChange Lightning Site-Directed Mutagenesis Kit (Agilent, #210519) was used according to manufacturer's indications.

Electrophoresis mobility shift assay (EMSA)

DNA binding affinity of POLγA and POLγA-B2 to a primer-template was assayed using a 36-nucleotide (nt) oligonucleotide [5′-TTTTTTTTTTATCCGGGCTCCTCTAGACTCGACCGC-3′] annealed to a ^{32}P 5′-labeled 21-nt complementary oligonucleotide (5′-GCGGTCGAGTCTAGAGGAGCC-3′). This produces a primed-template with a 15 bases single-stranded 5′-tail. Reactions were carried out in 15 µl volumes containing 10 fmol DNA template, 20 mM Tris-HCl [pH 7.8], 1 mM DTT, 0.1 mg/ml bovine serum albumin, 10 mM $MgCl_2$, 10% glycerol, 2 mM ATP, 0.3 mM ddGTP and 3 mM dCTP. POLγA and POLγB were added as indicated in the figures and reactions were incubated at RT for 10 min before separation on a 6% Native PAGE gel in 0.5 X TBE for 35 min at 180V. Bands were visualized by autoradiography.

For K_d analysis, band intensities representing unbound and bound DNA were quantified using Multi Gauge V3.0 software (Fujifilm Life Sciences). The fraction of bound DNA was determined from the background-subtracted signal intensities using the expression: bound/(bound+unbound). The fraction of DNA bound in each reaction was plotted versus the concentration of POLγA or POLγA-B2. Data were fit using the "one site – specific binding" algorithm in Prism 8 (Graphpad Software) to obtain values for K_d.

Coupled exonuclease-polymerase assay

DNA polymerization and 3′-5′ exonuclease activity were assayed using the same primer-template as described above for EMSA. The reaction mixture contained 10 fmol of the DNA template, 25 mM Tris-HCl [pH 7.8], 10% glycerol, 1 mM DTT, 10 mM $MgCl_2$, 100 µg/ml BSA, 60 fmol of POLγA, 120 fmol of POLγB and the indicated concentrations of the four dNTPs. The reaction was incubated at 37 °C for 15 min and stopped by the addition of 10 µl of TBE-UREA-sample buffer (BioRad). The samples were analysed on a 15% denaturing polyacrylamide gel in 1 X TBE buffer.

DNA synthesis on ssDNA template

A ^{32}P 5′-labeled 70-mer oligonucleotide [5′-42(T)-ATCTCAGCGATCTGTCTATTTCGTTCAT-3′] was hybridized to a single-stranded pBluescript SK(+). The template formed consists of a 42 nt single-stranded 5′-tail and a 28 bp duplex region. Reactions were carried out in 20 µl volumes containing 10 fmol template DNA, 25 mM Tris-HCl (pH 7.8), 1 mM DTT, 10 mM $MgCl_2$, 0.1 mg/ml BSA, 100 µM dATP, 100 of the four dNTPs, 2.5 pmol mtSSB, 150 fmol POLγA and 300 fmol POLγB. Reactions were incubated at 37 °C for the indicated times and stopped by the addition of 6 µl of stop buffer (90 mM EDTA, 6% SDS, 30% glycerol, 0.25% bromophenol blue and 0.25% xylene cyanol) and separated on a 0.9% agarose gel at 130V in 1× TBE for 4h.

Rolling circle *in vitro* replication assay

A ^{32}P 5′-labeled 70-mer oligonucleotide [5′-42(T)-ATCTCAGCGATCTGTCTATTTCGTTCAT-3′] was hybridized to a single-stranded pBluescript SK(+) followed by one cycle of polymerization using KOD polymerase (Novagen) to produce a ~3-kb double-stranded template with a preformed replication fork. Reactions of 20 µl were carried out containing 10 fmol template DNA, 25 mM Tris-HCl (pH 7.8), 1 mM DTT, 10 mM $MgCl_2$, 0.1 mg/ml BSA, 4 mM ATP, 100 µM dATP, 100 µM dTTP, 100 µM dGTP, 10 µM dCTP, 2 µCi [α-^{32}P] dCTP, 2 pmol mtSSB, 200 fmol TWINKLE, 200 fmol POLγA and 500 fmol POLγB (or as indicated in the figure). Reactions were incubated at 37 °C for 60 min (or as indicated in the figure) and stopped with 6 µL alkaline stop buffer (18% [wt/vol] Ficoll, 300 mM NaOH, 60 mM EDTA [pH8], 0.15% [wt/vol] Bromocresol green, and 0.35% [wt/vol] xylene cyanol). Products were run in 0.8% alkaline agarose gels and visualized by autoradiography. Incorporation of [α-^{32}P]-dCTP was measured by spotting 5 µl aliquots of the reaction mixture (after the indicated time points at 37 °C) on Hybond N+ membrane strips (GE Healthcare Lifesciences). The membranes were washed (3 × with 2 × SSC and 1 × with 95% EtOH) and the remaining activity was quantified using Multi Gauge V3.0 software (Fujifilm Life Sciences). A dilution series of known specific activity of [α-^{32}P]-dCTP was used as a standard.

Thermofluor assay

The fluorescent dye Sypro Orange (Invitrogen) was used to monitor the temperature-induced unfolding of wild-type and mutant POLγA as

previously described (31). Briefly, wild-type and mutant proteins were set up in 96-well PCR plates at a final concentration of 1.6 µM protein and 5 × dye in assay buffer (50 mM Tris-HCl pH 7.8, 10 mM DTT, 50 mM $MgCl_2$ and 5 mM ATP). Differential scanning fluorimetry was performed in a C1000 Thermal Cycler using the CFX96 real time software (BioRad). Scans were recorded using the HEX emission filter (560-580 nm) between 4 and 95 °C in 0.5 °C increments with a 5 seconds (s) equilibration time. The melting temperature (Tm) was determined from the first derivative of a plot of fluorescence intensity versus temperature (32). The standard error was calculated from 3 independent measurements.

LONP1 proteolysis assay

Protease activity of purified LONP1 on POLγA was measured in a 15 µl reaction volumes containing 0.5 µg of LONP1 wild-type and 0.55 µg of POLγA (in presence or absence of 0.22 ug of POLγB). When having both POLγA and POLγB in the same reaction, a preincubation in ice for 10 min is made before adding LONP1 to the reaction. Samples were incubated at 37 °C for 0-90 min in a buffer containing 50 mM Tris-HCl pH 8.0, 10 mM $MgCl_2$, 0.1 mg/ml BSA, 2 mM ATP and 1 mM DTT and the reactions were stopped by addition of Laemli sample buffer (BioRad). Samples were run on precast 4-20% gradient SDS-PAGE gels (BioRad, 567-8094) and visualized using ImageLab™ (BioRad) to detect proteolytic activity on POLγA. Band intensities were measured with ImageLab™ (BioRad) and calculations were made in order to provide %

remaining POLγA-values. Reactions and calculations were made in triplicate and SD was calculated.

Gel filtration analysis

Complex formation between POLγA and POLγB was tested by size-exclusion chromatography using a Superose 6 Increase 10/300 column (GE Healthcare) connected to an ÄKTA Purifier (GE Healthcare). The column was equilibrated in buffer D (25 mM Tris–HCl, pH 7.8, 10% glycerol, 1 mM DTT, 0.5 M NaCl, 10 mM $MgCl_2$). Equal amounts (1 nmoles) of POLγA and POLγB were pre-incubated in buffer D for 10 min on ice before injection. Samples (200 µl) were injected onto the column through a 200 µl loop and run at 1ml/min. Fractions of 250 µl were collected and analyzed on a precast 4-20% gradient SDS-PAGE gel and visualized using ImageLab™ (BioRad). A size calibration curve was previously prepared using thyroglobulin (670 kDa), c-globulin (158 kDa), ovalbumin (44 kDa), myoglobin (17 kDa) and vitamin B12 (1.35 kDa) according to the manufacturer's instructions (BioRad, 151-1901).

To analyze the LONP1 ^{S855A} -POLγA interaction, a home-made gel filtration column (0,5 cm x 30 cm) was prepared using Bio-Gel agarose with a bead size of 75-150 µm (BioRad, 151-0440) and calibrated using a gel filtration standard (BioRad, 151-1901). Preincubation of the proteolytic mutant of LONP1 with POLγA in the presence of 2 mM ATP and 10 mM $MgCl_2$ at 37 °C for 10 min allowed the formation of the

complex that was later injected into the column and eluted in 1 CV of buffer D. Fractions of 200 µl were collected and analyzed in a precast 4-20% gradient SDS-PAGE gel and visualized using ImageLab™ (BioRad).

Statistical analysis

All numerical data are expressed as mean ± SEM unless otherwise stated. A two tailed Student's *t*-test was used to assess statistical significance (see figure legends for details) in two groups comparisons. Two-way ANOVA test with Tukey's correction was used for multiple comparisons. Differences were considered statistically significant for $p < 0.05$. Animals were randomized in treated and untreated groups. No blinding to the operator was used.

Results

Generation and characterization of *Polg*$^{A449T/A449T}$ mutant mice

To investigate the molecular pathogenesis of *POLG*-related disorders, we generated a *Polg*$^{A449T/A449T}$ homozygous knockin mouse, corresponding to the human A467T mutation, by CRISPR/Cas9 technology (Supplementary Figure 1). Three-month old *Polg*$^{A449T/A449T}$ homozygous animals did not show any gross phenotype compared to wild-type (WT) littermates, including similar body weight curve and rotarod performance (not shown). However, a 19.6 % ($p < 0.05$) reduction in treadmill motor endurance and in the rearing activity in the cages was detected (Figure 1A). Although whole body metabolism was similar

in KI and controls by CLAMS analysis, a 41% ($p < 0.05$) reduction in spontaneous rearing movements was observed in *Polg*$^{A449T/A449T}$ mutants (Figure 1B-C and Supplementary Figure 2). Aged, one-year-old *Polg*$^{A449T/A449T}$ homozygous animals were very similar to the 3-month-old mice ruling out a late onset phenotype (Supplementary Figure 3A-B). Post-mortem hematoxylin and eosin staining at both ages did not show any gross abnormality in any tissue (Supplementary Figure 4). We monitored the *Polg*$^{A449T/A449T}$ and WT littermates up to two years of age, but neither reduction of the lifespan nor the presence of obvious age-related phenotypes was observed. Therefore, we focused our analysis on 3-month-old animals, unless otherwise stated.

POLγA is reduced in *Polg*$^{A449T/A449T}$ tissues

We analysed the effects of the A449T mutation on POLγA and POLγB protein levels. Immunoblotting revealed a strong reduction of POLγA^{A449T} amount, as low as 50%, in all tissues examined, including liver, skeletal muscle, brain, kidney and heart (Figure 2A-B). In contrast, POLγB levels were unchanged in most tissues, albeit a mild upregulation and downregulation in brain and heart, respectively, was observed (Figure 2A-C). Analysis of the corresponding mRNAs showed no significant changes of *Polg* or *Polg2* transcripts in both liver and skeletal muscle of *Polg*$^{A449T/A449T}$ compared to control littermates (Figure 2D-E), suggesting post-translational instability of the mutant protein.

Reduced mtDNA content and impaired replication in *Polg*$^{A449T/A449T}$ tissues and MEFs

Since mutations in *POLG* are associated with mtDNA instability in human patients, we next investigated mtDNA content and integrity in several tissues, including liver, skeletal muscle, brain, kidney and heart from both *Polg*$^{A449T/A449T}$ vs. WT littermates (Figure 3A). MtDNA copy number was significantly reduced in the skeletal muscle of 3-month-old *Polg*$^{A449T/A449T}$ (80±4%, $p<0.01$) compared to WT littermates, without accumulation of multiple deletions (Figure 3B and Supplementary Figure 5A-C). No difference in mitochondrial transcripts and OXPHOS activities were detected between *Polg*$^{A449T/A449T}$ vs. WT littermates in liver and SKM (Supplementary Figure 5D-J). Multiple deletions were also not detected in tissues of 1-year old *Polg*$^{A449T/A449T}$ homozygous animals and mtDNA quantifications were very similar to that of the 3-month old mice, except that in addition to skeletal muscle, a mild decrease in mtDNA copy number was also observed in kidney (79±6%, $p<0.01$) and heart (87±3%, $p<0.01$) (Supplementary Figure 3C-H).

To investigate in detail the effects on mtDNA replication we generated mouse embryonic fibroblasts (MEFs) from *Polg*$^{A449T/A449T}$ and WT cells. The mtDNA content was similar in the two genotypes (Supplementary Figure 5K). We then investigated mtDNA replication in MEFs, using 5-ethynyl-2′-deoxyuridine (EdU) staining in junction with an anti-DNA antibody to label replicating and total mtDNA. Interestingly, we observed a significantly increased fraction of replicating mtDNA molecules in *Polg*$^{A449T/A449T}$ vs. WT MEFs (Figure 3C-

F), indicating that more mtDNA foci were engaged in replication. Next, we used ethidium bromide (EtBr) to deplete mtDNA content, and found that after removal of EtBr, mtDNA content recovered to pre-treatment values within 3 days in WT MEFs, whereas no recovery at all was observed in the mutant cells (Figure 3G), strongly indicating severely impaired mtDNA replication in stress conditions of *Polg*$^{A449T/A449T}$ mouse mitochondria.

Given the mild reduction in mtDNA copy number in the mutant mice, we decided to challenge them with a single injection of carbon tetrachloride (CCl_4), which induces acute liver damage, triggering liver cell division to repopulate the necrotic areas. Two days after the injection, both WT and *Polg*$^{A449T/A449T}$ showed extensive areas of necrosis (approximatively 35% of the liver), which was reduced to 6±0.46 % in WT mice after four days, whereas it was still above 10% in *Polg*$^{A449T/A449T}$ mice (10±1.15%, $p<0.05$) (Figure 3H-I). This result clearly indicates that cell replication is impaired in *Polg*$^{A449T/A449T}$, likely due to lack of bioenergetic supply by impaired mitochondria in stress conditions. Since the antiepileptic drug valproic acid (VPA) is known to induce acute liver failure in patients with the A467T mutation in POLγA (33,34), we treated our mice with VPA by daily oral gavage (300 mg/kg) for one week or in food pellets (1.5% VPA) for two months. Both WT and *Polg*$^{A449T/A449T}$ did not show any sign of hepatic failure or histological damage.

Polg$^{A449T/A449T}$ mitochondria have reduced 7S DNA and accumulate replication intermediates

We then investigated mtDNA replication in the tissues of the mutant and control mice by Southern blot. Normally, about 95% of all replication events are prematurely terminated, generating a 650 nucleotide-long molecule, called 7S DNA (35-37). In *Polg*$^{A449T/A449T}$ but not in WT littermate, the 7S DNA levels were significantly reduced in skeletal muscle and kidney, and a similar trend was also present in the other analysed tissues, except for the heart, (Figure 4A-B and Supplementary Figure 6A-C). These results suggest compensatory mtDNA replication in knockin mice vs. WT littermates.

To better investigate the mechanistic details of mtDNA replication, we then performed *in organello* replication experiments in isolated liver mitochondria (Figure 4C), by pulse-labelling with α-^{32}P-dATP. Although no obvious differences were detected in mtDNA replication rates between *Polg*$^{A449T/A449T}$ and WT mice (Figure 4C), the signal due to long but incomplete mtDNA molecules was much more intense in the *Polg* mutant compared to WT samples, thus suggesting accumulation of replication intermediates (RIs) in the mutant vs. controls. Accordingly, we applied two-dimension agarose gel electrophoresis (2D-AGE), which resolves DNA molecules based on size and shape, allowing a snapshot of the RIs. Notably, *Polg*$^{A449T/A449T}$ mice displayed an overall accumulation of the different types of RIs compared to WT animals (Figure 4D and Supplementary Figure 6D-F), revealing abnormal replication of *Polg*$^{A449T/A449T}$ mainly due to generalized replication fork stalling.

These results are concordant with those found in MEFs (Figure 3C-F).

These novel data clearly demonstrate that the A449T mutation impairs mtDNA replication in both cultured cells and *in vivo*.

POLγA^{A449T} protein has reduced affinity for DNA and polymerase activity, which are partially rescued by POLγB subunit

To further document the stalling phenotype of the A449T mutant *in vitro*, we expressed and purified both human (h) and mouse (m) WT and mutant POLγA as recombinant proteins. First, we used an electrophoretic mobility shift assay (EMSA) to measure the binding of mPOLγA to a primed DNA template. When alone, mPOLγA^{A449T} bound DNA ≈ 3.4 times less than mPOLγA^{WT} (Figure 5A and Supplementary Figure 7A) and remained 1.75 times lower than the WT also after the addition of POLγB (Figure 5B and Supplementary Figure 7B).

Next, we investigated mPOLγA activities using a short DNA template annealed to a radioactively labelled primer. By performing the experiment across a range of dNTP concentrations, we could analyze both polymerase and exonuclease function. The exonuclease activity can digest the labelled primer, whereas the polymerase activity can elongate the primer and synthesize an additional short, 15 nucleotide-stretch of DNA. As expected, at lower dNTP levels, mPOLγA^{wt} displayed 3′-5′ exonuclease activity, but at higher concentrations, it switched to polymerase activity (Figure 5C). Addition of mPOLγB reduced exonuclease activity and favored DNA synthesis even at lower dNTP concentrations (Figure 5D). The mutant mPOLγA^{A449T} was completely inactive in isolation, most likely due to its inability to

efficiently bind primed DNA (Figure 5C). Nevertheless, addition of mPOLγB restored the polymerase activities of mPOLγA^{A449T}, to levels similar to those observed with mPOLγA^{wt} (Figure 5D), whereas exonuclease activity was reduced also in mPOLγA^{wt} as a consequence of predominant polymerase activity measured *in vitro* (Figure 5D).

To further challenge the system, we performed a DNA synthesis assays using a long circular ssDNA template of 3000 nt (Figure 5E). mPOLγA^{A449T} displayed a clearly slower DNA synthesis rate compared to the mPOLγA^{WT}, even in the presence of the mPOLγB subunit (Figure 5F).

To monitor the effects of the A449T mutation on replication of dsDNA, we used a template containing a ~4 kb long dsDNA region with a free 3′-end acting as a primer (Figure 5G). Addition of the TWINKLE DNA helicase was required to unwind the DNA and the reaction was stimulated by mtSSB (Figure 5G). This reaction is absolutely dependent on POLγB and once initiated, very long stretches of DNA can be formed. In this rolling circle replication assay, mPOLγA^{A449T} showed reduced polymerase DNA synthesis rate (Figure 5H) compared to mPOLγA^{WT}, at all concentrations tested (Supplementary Figure 7C), demonstrating that mPOLγA^{A449T} has reduced polymerase activity. This *in vitro* result is in perfect agreement with the stalling phenotype seen *in vivo*. A similar effect was obtained with the hPOLγA^{A467T} (Figure 5I).

Analysis of incorporated radiolabelled nucleotides over time indicated that the *in vitro* replication rates with 10 μM dNTPs, were reduced to about 60% for mPOLγA^{A449T} compared to mPOLγA^{WT} (3.5 fmol/min

vs 5.5 fmol/min) (Supplementary Figure 7D-E). Interestingly, the reduction was more pronounced with hPOLγA^{A467T} compared to hPOLγA^{WT} (1.4 fmol/min vs 5.3 fmol/min), than for the mouse equivalents, which could explain the more severe phenotype observed in patients (Supplementary Figure 7D-E).

POLγA is unstable in absence of POLγB

The amount of mPOLγA^{A449T} was reduced in the *Polg*$^{A449T/A449T}$ mice, which could also contribute to impaired mtDNA replication. To better understand the impact of the A449T mutation on protein stability, we performed a thermofluor stability assay and monitored temperature-induced unfolding of mPOLγA^{WT} and mPOLγA^{A449T}, both in absence and in presence of mPOLγB (Figure 6A and 6B). The stability assay revealed no major differences in the fluorescence profile between mPOLγA^{WT} and mPOLγA^{A449T} from 37 °C upwards, but the fluorescence signal of mPOLγA^{A449T} was already higher than the WT at 25 °C, clearly indicating that the mutant protein was already partially unfolded even at <37 °C temperatures (Figure 6A and 6B). Interestingly, the presence of the mPOLγB had a dramatic stabilizing effect, by increasing the unfolding temperature of about 10 °C for both proteins (Figure 6A and 6B). These data suggest that POLγA^{WT} is also partially unstable in the absence of POLγB. Accordingly, a recent report demonstrated that human POLγB-knockout cells showed severe decrease in POLγA levels (38).

We hypothesized that the A449T mutation could impair interactions with mPOLγB and thus destabilize mPOLγA^{A449T}. The A449 (mouse)/A467 (human) residue is located in the thumb helix that forms contacts with POLγB. The mutation disrupts the local hydrophobic environment formed by L466 and L602. As a consequence, there is a slight spatial shift of the thumb domain, which could potentially disturb binding to POLγB. (Supplementary Figure 8A) (39). To address this possibility, we investigated mPOLγA^{A449T} interactions with mPOLγB by performing size-exclusion chromatography. At 1:1 molar ratio of mPOLγA and mPOLγB (calculated as a dimer), mPOLγ^{WT} and mPOLγB migrated as a single peak, corresponding to a stable complex between the two proteins (Figure 6C), as confirmed by SDS-PAGE (Figure 6D). In contrast, mPOLγA^{A449T} and mPOLγB showed an additional peak, corresponding to unbound mPOLγB (Figure 6C and 6E). The resolution of the chromatography cannot separate free POLγA from the POLγ holoenzyme. Thus, the A449T mutation significantly reduces the interaction between POLγA and POLγB subunits. This observation is in agreement with data for hPOLγA^{A467T} (11).

POLγB protects POLγA against LONP1 degradation

Next, we investigated if free, partially unfolded POLγA could be a target for protein degradation. The LONP1 protease degrades misfolded proteins in mitochondria and has previously been linked to regulation of mtDNA copy number (40). We decided to investigate if POLγA was a target for LONP1.

We first used siRNA interference against LONP1, POLγA and POLγB in HeLa cells. Interestingly, LONP1 knockdown caused a robust increase in POLγA levels (Figure 6F and 6G), whereas POLγB was unaffected (Figure 6F), supporting the idea that POLγA, but not POLγB, is a specific target for LONP1 degradation. In agreement with a stabilizing effect of POLγB, knockdown of *Polg2* mRNA also caused a reduction of POLγA levels (Figure 6F and 6H). Both POLγB and POLγA knockdown resulted in an increase of LONP1 (Figure 6F). We also evaluated the steady state levels of POLγA in a heart-specific *Lonp1*$^{-/-}$ mouse model (6I and 6J). Notably, POLγA levels were increased in heart samples of *Lonp1*$^{-/-}$ compared to control littermates. Collectively, these results support that LONP1 specifically targets POLγA both in cells and *in vivo*.

To investigate if POLγA is a direct target for LONP1 degradation, we performed a size-exclusion chromatography with recombinant protein to assess if mouse POLγA can form a complex with LONP1. To ensure that POLγA was not degraded by LONP1 during the experiment, we used the mutant LONP1^{S855A}, which traps substrates without degrading them (41). As shown in Figure 7A, we observed a co-elution of LONP1^{S855A} and POLγA, revealing an interaction between these two proteins.

We also monitored LONP1 dependent degradation of POLγA and POLγB *in vitro*. We followed the reactions over time and used another well-characterized LONP1 substrate, TFAM, as a positive control (21,42). The TFAM levels were reduced by 50% in about 3 minutes (Figure 7B).

Mouse POLγB was not degraded by LONP1, confirming that the accessory subunit is not a substrate of the protease (Figure 7C, lanes 7-10). In contrast, both isolated mPOLγA^{WT} and mPOLγA^{A449T} were efficiently degraded, with a 50% reduction in about 20 minutes (Figure 7C, lanes 2-5, 7D, lanes 2-5 and 7E). The slower degradation time compared to TFAM could in part be explained by the size difference between the two substrates, with POLγA being about 6-fold larger. LONP1 is an ATP-dependent enzyme, and no degradation of POLγA was therefore observed in the absence of ATP (Figure 7C, lanes 1, 6 and 11).

Next, we examined POLγA in complex with POLγB. Interestingly, the presence of POLγB completely blocked POLγA^{wt} degradation (Figure 7C, lanes 12-15 and Figure 7E). In contrast, POLγB was unable to efficiently block degradation of POLγA^{A449T} and the levels of the mutant protein decreased significantly over the time of the experiment (Figure 7D, compare lanes 7-10 with 12-15 and Figure 7E). We also used the human WT and A467T mutant versions of POLγA, and obtained similar results (Figure 7F, 7G and 7H). We conclude that the impaired interaction between POLγB and POLγA^{A449T} leads to increased LONP1-dependent degradation of POLγA^{A449T}. This observation could explain the lower levels of POLγA^{A449T} observed *in vivo*.

To validate our model, we also analysed two additional POLγA mutations. The mouse version of POLγA^{W748S} (POLγA^{W725S}), which also displays reduced interactions with POLγB (Supplementary Figure 9A-C) and human POLγA^{D274A}, which has no effect on POLγB interactions

(43). As expected, mPOLγA^{W725S} but not hPOLγA^{D274A} was degraded in presence of POLγB (Supplementary Figure 9D-F).

Our observations *in vitro* implied that the POLγB dimer must be present in at least stoichiometric amounts *in vivo* to prevent POLγA degradation. To determine the *in vivo* ratio of the two proteins, we performed quantitative immunoblotting using polyclonal antibodies against the POLγA and POLγB in various mouse tissues (kidney, liver, brain, skeletal muscle, heart) and human HeLa cells. Protein levels were determined by comparison with known amounts of recombinant POLγA and POLγB. As predicted, the levels of the POLγB dimer was higher than POLγA in all cell types investigated. The ratio varied between 4:1 and 15:1 of the POLγB dimer relative POLγA (Supplementary Figure 8B-E). Overall, these data provide evidence that POLγB affects POLγA folding and protects the protein from degradation. Our data also suggest that other POLγA mutations affecting the interactions with POLγB or vice versa (e.g. mutations in POLγB affecting the interaction with POLγA) may be subjected to LONP1 degradation.

Discussion

Mutations in *POLG* are a relatively common cause of a spectrum of mitochondrial disease. The substantial lack of relevant *in vivo* models has hampered our understanding of the pathogenesis of these *POLG*-related disorders. Here we developed a mouse model for human POLG^{A467T} and study the molecular pathogenesis of this common mutation

in vivo. We complemented this analysis with detailed biochemical characterization of the corresponding events *in vitro*.

The mouse model revealed a clear effect on mtDNA replication in homozygous *Polg*$^{A449T/A449T}$ mice compared to wt controls. In mutant mouse tissues, we observed a reduction of 7S DNA and increased levels of replication intermediates. Similar effects have previously been described in knock-out models for other components of the mitochondrial replication machinery, including POLγB (44); mtSSB (45); and TWINKLE (46). In addition, experiments carried out on *Polg*$^{A449T/A449T}$ MEFs revealed a striking reduction of mtDNA recovery after depletion with EtBr, thus demonstrating that POLγ activity is severely impaired in the mouse model, similar to what was described in human fibroblasts harboring distinct POLγ mutations (47). Surprisingly, despite these clear biochemical consequences, the mutant mouse model displayed very mild phenotypes compared to patients. We observed no reduction of lifespan or any obvious age-related phenotypes. In addition, the mutant mice were resilient to various challenges, including administration of valproate. The only obvious phenotype seen was after administration of CCl_4, which resulted in a slightly reduced recovery rate to liver damage, demonstrating that effective mtDNA replication is necessary for liver regeneration. Similar results have previously been reported for a knockout mouse model of mitochondrial topoisomerase I (TOP1mt) (48). Although we do not have an obvious explanation for the phenotypic differences between POLγ-defective mice and patients, our

results suggest that the mutant mice may have effective compensatory mechanisms which mitigates POLγ dysfunction.

In agreement with the effect on mtDNA replication observed *in vivo*, our analysis of mPOLγA^{A449T} *in vitro* revealed a decrease in exonuclease and polymerase activities, which were partially rescued in the presence of POLγB. This observation highlights the importance of POLγB for the activity of POLγA. Interestingly, a comparison between the mouse POLγA^{A449T} and human POLγA^{A467T} proteins, revealed similar but more pronounced replication defects for the human polymerase, which can also help to explain why the human A467T mutation causes more severe phenotypes in affected patients (Figure 5H and I and Supplementary Figure 7C-D. These findings also demonstrate that the mouse model reproduces the molecular signature of the human disease, despite the milder phenotypes observed.

Interestingly, we noticed a reduction of POLγA^{A449T} protein levels in mouse tissues, and thus investigated the possible causes of this reduction. Using a thermofluor stability assay, we found that in isolation, POLγA is structurally unstable at physiological temperatures, but strongly stabilized in complex with POLγB. Size-exclusion chromatography demonstrates that the A449T mutation impairs interactions between POLγA and POLγB, disturbing POLγ holoenzyme formation. This latter observation is supported by structural modeling of A449T, which is situated in a region of POLγA

required for interactions with POLγB. In our thermofluor analysis, we also noted a slight destabilization of POLγA^{A449T} at lower temperatures. Guided by these observations, we hypothesized that POLγA^{A449T} is a target for LONP1, a mitochondrial protease that degrades misfolded proteins.

The idea that POLγA^{A449T} is a substrate of LONP1 and that POLγB serves as a stabilizing, protective factor, were supported by both *in vitro* biochemical evidence and *in vivo* observations. Notably, depletion of LONP1 causes an increase POLγA levels in both mouse tissues and human cells. In contrast, depletion of POLγB leads to lower levels of POLγA, whereas depletion of POLγA has no discernible effect on POLγB. In this context, it should be noted that we cannot rule out that other proteases can contribute to POLγA degradation *in vivo* (49).

In addition, the superstoichiometric levels of POLγB relative to POLγA in human cells and mouse tissues, also supports the idea that POLγB protects POLγA from proteolysis. The rapid degradation of POLγA in the absence of POLγB could be of physiological relevance, since on its own, the POLγA displays low polymerase activity but high exonuclease activity, which may disturb mtDNA replication.

In our experiments, we noted that depletion of either POLγA or POLγB resulted in increased levels of LONP1. The exact cause of this effect

is unclear, but LONP1 has many other targets in vivo and is required for multiple mitochondrial functions. We therefore hypothesize that the increase is a part of a more general stress response, similar to what has been suggested previously (50).

Furthermore, during analysis, we also noted that native POLγB run at a slightly higher molecular weight than expected. The reason for the difference between the predicted and observed size of the protein is not known to us, but could indicate that the cleavage site for the leader peptide is different from what has previously been predicted in the literature. Alternatively, POLγB may contain post-translational modifications that affect its migration in SDS-PAGE. Clarifying this point warrants additional work and may have consequences for our understanding of POLγ function.

In conclusion, we here describe in detail the *in vivo* and *in vitro* features of a common POLγA mutation, with potential implications for the pathogenesis of a previously poorly understood condition. Our findings imply that mutations in *POLG1* or *POLG2* that cause weaker interactions within the POLγ holoenzyme will lead to degradation of POLγA, resulting in protein depletion *in vivo*. We speculate that interventions aimed at increasing POLγA stability, either by directly stabilising the protein or increasing interactions with POLγB may have therapeutic value in affected patients.

Data availability

The data that support the findings of this work are available from the corresponding authors upon request

Supplementary Data

Supplementary Data are available at NAR Online.

Acknowledgements

The authors would like to thank Jay P Uhler for generating the graphical abstract

Funding

Our research is supported by the Telethon Foundation (grant GGP19007 to MZ), NRJ-Institute de France Grant (to M.Z.), Fondazione Onlus Luigi Comini (to MZ and CV); and core grants from the Medical Research Council (Grant MC_UU_00015/5, MC_UU_00015/4 and MC_UU_00015/7). PSP, CPH and DHH are supported by the Marie Sklodowska-Curie ITN-REMIX grant (Grant 721757), the Swedish Research Council (MF); Swedish Cancer Foundation (MF); European Research Council (MF); the Knut and Alice Wallenbergs Foundation (MF). LT is supported by a MRC-funded graduate student fellowship. SAD is supported by EMBO Installation Grant IG4149, TUBITAK 119C022 and Bogazici University SUP-15501.

Conflict of Interest Disclosure

The authors have no competing interests to disclose

Figure Legends

Figure 1. Characterization of the clinical phenotype of *Polg*$^{A449T/A449T}$ mice.

A. Distance run in metres by 3 month-old WT and *Polg*$^{A449T/A449T}$ animals on the treadmill. Data are presented as mean ± SEM. *p<0.05; Student's t-test. Each symbol represents a biological replicate.

B. Spontaneous rear activity (vertical movement counts) of 3 month-old WT and *Polg*$^{A449T/A449T}$ animals measured in the CLAMS™ system. Data are presented as mean ± SEM. Two tailed unpaired Student's *t*-test: *p<0.05; Each symbol represents a biological replicate.

C. Spontaneous ambulatory activity (horizontal movement counts) of 3 month-old WT and *Polg*$^{A449T/A449T}$ animals measured in the CLAMS™ system. Data are presented as mean ± SEM. Student's *t*-test. Each symbol represents a biological replicate.

Figure 2. Characterization of POLγA and POLγB levels in tissues of *Polg*$^{A449T/A449T}$ mice.

A. Western blot analysis of steady-state levels of POLγA and POLγB in liver, skeletal muscle (SKM), kidney, brain and heart of WT and *Polg*$^{A449T/A449T}$ animals. The lower band in the brain is unspecific. GAPDH was used as loading control. Each lane represents a biological replicate.

B-C. Quantification of (**A**). POLγA (**B**) and POLγB (**C**) levels were normalized to GAPDH and presented as FOLD change from WT animals.

Data are presented as mean ± SEM. Two tailed unpaired Student's *t*-test: *p<0.05; **p<0.01; ***p<0.001; ****p<0.0001. Each symbol represents a biological replicate.

D-E. Real-Time qRT-PCR quantification of the transcripts *Polg* **(D)** and *Polg2* **(E)**, normalized to *B2m*, in liver and skeletal muscle (SKM) of WT and *Polg*$^{A449T/A449T}$ animals. Data are presented as mean ± SEM. Two tailed unpaired Student's *t*-test: non significant. Each symbol represents a biological replicate.

Figure 3. Characterization of the molecular phenotype of *Polg*$^{A449T/A449T}$ mice.

A. Real-Time qPCR quantification of mtDNA content in liver, skeletal muscle (SKM), kidney, brain and heart of WT and *Polg*$^{A449T/A449T}$ animals. Data are presented as mean ± SEM. Two tailed unpaired Student's *t*-test: **p<0.01. Each symbol represents a biological replicate.

B. Long-range PCR performed in DNA isolated from skeletal muscle (SKM) and liver of WT and *Polg*$^{A449T/A449T}$ animals. Primers amplifying a fragment of 15,781bp of the mtDNA. The bands were visualized by SYBR™ safe staining. Each lane represents a biological replicate.

C. Representative confocal images of mitochondria, DNA and replicating mtDNA (EdU) from WT and *Polg*$^{A449T/A449T}$ MEFs. Mitochondria and mtDNA were labelled using anti-TOM20 and anti-DNA antibodies, respectively. Replicating DNA was visualized in fixed cells after incubation with 50 µM EdU for 1 hour . Scale bar 20 µm.

D. Quantification of total mtDNA from (**A**). Data are presented as mean ± SEM. Two tailed unpaired Student's *t*-test: p= non significant. Each symbol represents individual cells (n=60) from three independent experiments.

E. Quantification of mitochondrial EdU positive foci from (**A**). Data are presented as mean ± SEM. Two tailed unpaired Student's *t*-test: ***p<0.001. Each symbol represents individual cells (n=60) from three independent experiments.

F. Ratio of the mitochondrial replicating mtDNA / total mtDNA. Data are presented as mean ± SEM. Two tailed unpaired Student's *t*-test: **p<0.01. Each symbol represents individual cells (n=60) from three independent experiments.

G. Real-Time qPCR quantification of mtDNA content in WT and *Polg*$^{A449T/A449T}$ MEFs during Ethidium Bromide-mediated depletion and then recovery of mtDNA. Data are presented as mtDNA percentage (%) of untreated cells of each genotype. Data are presented as mean ± SEM. (n = 3).

H. Representative H&E staining of liver tissue sections of WT (top) and *Polg*$^{A449T/A449T}$ (bottom) animals with a single injection of CCl_4. Two days after injection (middle), 4 days after injection (right) and control/non-injected mice (left). Note the necrotic areas around the central veins (highlighted with black lines at day 4). Scale bar 100 µm.

I. Quantification of necrotic areas (D) as percentage (%) of the total section area, 2 and 4 days after a single injection of CCl_4.

Data are presented as mean ± SEM. Two tailed unpaired Student's *t*-test: *p<0.05. Each symbol represents a biological replicate.

Figure 4. Molecular analysis of mtDNA replication in *Polg*$^{A449T/A449T}$ mitochondria.

A. Southern blot analysis of BlpI-digested mtDNA and 7S DNA from skeletal muscle (SKM) and liver of WT and *Polg*$^{A449T/A449T}$ animals.

B. Quantification of the Southern blots presented in panel A and Supplemental Figure 4A-C. 7S DNA levels were normalized to linearized full length mtDNA and presented as FOLD change from WT animals. Data are presented as mean ± SEM. Two tailed unpaired Student's *t*-test: *p<0.05; **p<0.01. Each symbol represents a biological replicate.

C. Time course of *de novo* DNA synthesis of mtDNA, 7S DNA and RIs in liver-isolated mitochondria of WT and *Polg*$^{A449T/A449T}$ animals. Brackets indicate mtDNA replication intermediates (RIs). Pulse-labelling time (minutes) is indicated on the top.

D. Analysis of the mtDNA replication intermediates (RIs) in the liver of WT and *Polg*$^{A449T/A449T}$ mice, resolved by 2D-AGE and followed by southern blot visualization. DNA was digested with the BclI restriction enzyme. For probe and restrictions sites location, schematic representation and quantification of the different types of RIs, please refer to (Supplemental Figure 4D-F).

Figure 5. *In vitro* characterization of POLγA^{A449T} mutant protein.

A. Electrophoretic mobility assays using POLγA^{WT} and mutant POLγA^{A449T} to estimate affinity to a DNA template. For Kd (DNA) calculations please refer to (Supplemental Figure 5A). Each lane contains 10 fmol of DNA substrate and the indicated amounts of POLγA on the top.

B. Electrophoretic mobility assays using POLγA^{WT} and mutant POLγA^{A449T} with addition of POLγB to estimate affinity to a DNA template. For Kd(DNA) calculations please refer to (Supplemental Figure 5B). Each lane contains 10 fmol of DNA substrate and the indicated amounts of POLγ holoenzyme on the top.

C. Coupled exonuclease-polymerase assay using POLγA^{WT}and mutant POLγA^{A449T} across increasing concentrations of dNTPs using a short DNA template. A schematic representation of the assay is presented on the left.

D. Coupled exonuclease-polymerase assay using POLγA^{WT} and mutant POLγA^{A449T} with addition of POLγB, across increasing concentrations of dNTPs using a short DNA template.

E. Schematic representation of the second strand synthesis assay. This assay evaluates the ability of polymerise long stretches of DNA by synthesising the second strand of a single stranded template hybridized with a 5′ radiolabelled primer. MtSSB is added in the reaction.

F. Second strand synthesis assay using WT and mutant POLγA^{A449T} to assess polymerase activity using longer DNA templates. The reactions

include POLγA-B2 and mtSSB and were incubated for the indicated times on top of the blot.

G. Schematic representation of the Rolling circle *in vitro* replication assay. The template consists of an incomplete double stranded DNA template with a mismatch on the 5′ of the incomplete strand. In the presence of TWINKLE and mtSSB, POLγA-B2 can polymerase long stretches of DNA using the 3′-end of the incomplete strand.

H. Rolling circle *in vitro* replication assay using POLγA^{WT} and mutant POLγA^{A449T} to assess polymerase activity in the context of the minimal mitochondrial replisome, which includes POLγ holoenzyme WT or mutant, TWINKLE and mtSSB). The reactions were incubated for the indicated times (top).

I. Rolling circle *in vitro* replication assay using human versions of POLγA^{WT} and mutant POLγA^{A467T} to assess polymerase activity in the context of the minimal mitochondrial replisome (POLγ holoenzyme WT or mutant, TWINKLE and mtSSB). The reactions were incubated for the indicated times (top).

Figure 6. Stability of POLγA^{A449T} mutant protein *in vitro* and *in vivo*.

A. Schematic representation of a typical thermofluor stability assay. This assay uses a fluorescent dye, SYPRO Orange, to monitor the temperature-induced unfolding of proteins. When the temperature starts to rise and unfold the protein, the SYPRO Orange dye fluoresces by binding to exposed hydrophobic patches.

B. Thermofluor stability assay to evaluate thermostability of POLγA^{WT} (black) and POLγA^{A449T} (blue), in absence (solid line) or presence (dashed line) of POLγB.

C. Size-exclusion chromatogram of POLγA^{WT} (black line) and POLγA^{A449T} (blue line) in presence of POLγB, to evaluate interaction between POLγA and POLγB.

D. SDS-PAGE of the selected peak fractions from (C) of POLγA^{WT} and POLγB.

E. SDS-PAGE of the selected peak fractions from (C) of POLγA^{A449T} and POLγB. Note the brackets highlighting unbound POLγB (free from POLγA^{A449T}).

F. Western blot analysis of steady-state levels of POLγA, LONP1 and POLγB upon siRNA-mediated knockdown of LONP1, POLγB and POLγA, in HeLa cells. ß-actin was used as loading control.

G. Quantification of POLγA levels upon siRNA-mediated knockdown of LONP1 (F). POLγA levels were normalized to ß-actin and presented as FOLD change from cells treated with control siRNA. Data are presented as mean ± SEM. Two tailed unpaired Student's *t*-test: ***p<0.001. (n = 3).

H. Quantification of POLγA levels upon siRNA-mediated knockdown of POLγB (F). POLγA levels were normalized to ß-actin and presented as fold change from cells treated with control siRNA. Data are presented

as mean ± SEM. Two tailed unpaired Student's *t*-test: ***p<0.001. (n = 3).

I. Western blot analysis of steady-state levels of POLγA in heart of *Lonp1*$^{+/+}$ and *Lonp1*$^{-/-}$ animals. An anti-LONP1 antibody was used to confirm gene knockout and HSC70 was used as loading control.

J. Quantification of POLγA levels in heart of *Lonp1*$^{+/+}$ and *Lonp1*$^{-/-}$ animals (I). POLγA levels were normalized to HSC70 and presented as fold change from *Lonp1*$^{+/+}$. Data are presented as mean ± SEM. Two tailed unpaired Student's *t*-test: *p<0.05. (n = 6).

Figure 7. POLγA is a target of LONP1 degradation *in vitro*.

A. Size-exclusion chromatography of the complex formed by LONP1^{S855A} (Catalytic dead mutant) and WT POLγA. The mixture was incubated for 10min, at 37 °C, in the presence of 10 mM $MgCl_2$ and 2 mM ATP before loaded on the chromatography.

B. SDS-PAGE of the LONP1 proteolysis assay of TFAM, over time. The reactions were incubated for the indicated times (top).

C. SDS-PAGE of the LONP1 proteolysis assay of isolated POLγA^{WT} (left) and POLγB (middle), and POLγA^{WT} complexed with POLγB, over time. The reactions were incubated for the indicated times (top). In the absence of ATP (-ATP control), LONP1 does not exert proteolysis.

D. SDS-PAGE of the LONP1 proteolysis assay of POLγA^{A449T} in absence (left) or presence (middle) of POLγB, over time. Reactions with WT

POLγA + POLγB (right) were added for reference. The reactions were incubated for the indicated times (top). In the absence of ATP (-ATP control), LONP1 does not exert proteolysis.

E. Quantification of POLγA degradation over time (0-90min) by LONP1, related to (C-D). POLγA^{WT} (black) and POLγA^{A449T} (blue), in absence (solid line) or presence (dashed line) of POLγB. Data are presented as mean ± SD. (n = 3).

F. SDS-PAGE of the LONP1 proteolysis assay of human POLγA^{WT} in absence (left) or presence (right) of POLγB, over time. The reactions were incubated for the indicated times (top). In the absence of ATP (-ATP control), LONP1 does not exert proteolysis.

G. SDS-PAGE of the LONP1 proteolysis assay of human POLγA^{A467T} in absence (left) or presence (right) of POLγB, over time. The reactions were incubated for the indicated times (top). In the absence of ATP (-ATP control), LONP1 does not exert proteolysis.

H. Quantification of human POLγA degradation over time (0-90min) by LONP1, related to (F-G). POLγA^{WT} (grey) and POLγA^{A449T} (blue), in absence (solid line) or presence (dashed line) of POLγB. Data are presented as mean ± SD. (n = 3).

1

2

3

References

1. Gustafsson, C.M., Falkenberg, M. and Larsson, N.G. (2016) Maintenance and Expression of Mammalian Mitochondrial DNA. *Annu Rev Biochem*, **85**, 133-160.
2. Longley, M.J., Prasad, R., Srivastava, D.K., Wilson, S.H. and Copeland, W.C. (1998) Identification of 5'-deoxyribose phosphate lyase activity in human DNA polymerase gamma and its role in mitochondrial base excision repair in vitro. *Proc Natl Acad Sci U S A*, **95**, 12244-12248.
3. Ropp, P.A. and Copeland, W.C. (1996) Cloning and characterization of the human mitochondrial DNA polymerase, DNA polymerase gamma. *Genomics*, **36**, 449-458.
4. Lim, S.E., Longley, M.J. and Copeland, W.C. (1999) The mitochondrial p55 accessory subunit of human DNA polymerase gamma enhances DNA binding, promotes processive DNA synthesis, and confers N-ethylmaleimide resistance. *J Biol Chem*, **274**, 38197-38203.
5. Spelbrink, J.N., Li, F.Y., Tiranti, V., Nikali, K., Yuan, Q.P., Tariq, M., Wanrooij, S., Garrido, N., Comi, G., Morandi, L. *et al.* (2001) Human mitochondrial DNA deletions associated with mutations in the gene encoding Twinkle, a phage T7 gene 4-like protein localized in mitochondria. *Nat Genet*, **28**, 223-231.
6. Korhonen, J.A., Gaspari, M. and Falkenberg, M. (2003) TWINKLE Has 5' -> 3' DNA helicase activity and is specifically stimulated by mitochondrial single-stranded DNA-binding protein. *J Biol Chem*, **278**, 48627-48632.
7. Ferrari, G., Lamantea, E., Donati, A., Filosto, M., Briem, E., Carrara, F., Parini, R., Simonati, A., Santer, R. and Zeviani, M. (2005) Infantile hepatocerebral syndromes associated with mutations in the mitochondrial DNA polymerase-gammaA. *Brain*, **128**, 723-731.
8. de Vries, M.C., Rodenburg, R.J., Morava, E., van Kaauwen, E.P., ter Laak, H., Mullaart, R.A., Snoeck, I.N., van Hasselt, P.M., Harding, P., van den Heuvel, L.P. *et al.* (2007) Multiple oxidative phosphorylation deficiencies in severe childhood multi-system disorders due to polymerase gamma (POLG1) mutations. *Eur J Pediatr*, **166**, 229-234.
9. Horvath, R., Hudson, G., Ferrari, G., Futterer, N., Ahola, S., Lamantea, E., Prokisch, H., Lochmuller, H., McFarland, R., Ramesh, V. *et al.* (2006) Phenotypic spectrum associated with mutations of the mitochondrial polymerase gamma gene. *Brain*, **129**, 1674-1684.
10. Nguyen, K.V., Sharief, F.S., Chan, S.S., Copeland, W.C. and Naviaux, R.K. (2006) Molecular diagnosis of Alpers syndrome. *J Hepatol*, **45**, 108-116.
11. Chan, S.S., Longley, M.J. and Copeland, W.C. (2005) The common A467T mutation in the human mitochondrial DNA polymerase (POLG) compromises catalytic efficiency and interaction with the accessory subunit. *J Biol Chem*, **280**, 31341-31346.
12. Uusimaa, J., Gowda, V., McShane, A., Smith, C., Evans, J., Shrier, A., Narasimhan, M., O'Rourke, A., Rajabally, Y., Hedderly, T. *et al.* (2013) Prospective study of POLG mutations presenting in children with intractable epilepsy: prevalence and clinical features. *Epilepsia*, **54**, 1002-1011.
13. Viscomi, C. and Zeviani, M. (2017) MtDNA-maintenance defects: syndromes and genes. *J Inherit Metab Dis*, **40**, 587-599.
14. Rahman, S. and Copeland, W.C. (2019) POLG-related disorders and their neurological manifestations. *Nat Rev Neurol*, **15**, 40-52.
15. DeBalsi, K.L., Longley, M.J., Hoff, K.E. and Copeland, W.C. (2017) Synergistic Effects of the in cis T251I and P587L Mitochondrial DNA Polymerase gamma Disease Mutations. *J Biol Chem*, **292**, 4198-4209.
16. Rajakulendran, S., Pitceathly, R.D., Taanman, J.W., Costello, H., Sweeney, M.G., Woodward, C.E., Jaunmuktane, Z., Holton, J.L., Jacques, T.S., Harding, B.N. *et al.* (2016) A

Clinical, Neuropathological and Genetic Study of Homozygous A467T POLG-Related Mitochondrial Disease. *PLoS One*, **11**, e0145500.

17. Tzoulis, C., Engelsen, B.A., Telstad, W., Aasly, J., Zeviani, M., Winterthun, S., Ferrari, G., Aarseth, J.H. and Bindoff, L.A. (2006) The spectrum of clinical disease caused by the A467T and W748S POLG mutations: a study of 26 cases. *Brain*, **129**, 1685-1692.
18. Pinti, M., Gibellini, L., Nasi, M., De Biasi, S., Bortolotti, C.A., Iannone, A. and Cossarizza, A. (2016) Emerging role of Lon protease as a master regulator of mitochondrial functions. *Biochim Biophys Acta*, **1857**, 1300-1306.
19. Larsson, N.G., Wang, J., Wilhelmsson, H., Oldfors, A., Rustin, P., Lewandoski, M., Barsh, G.S. and Clayton, D.A. (1998) Mitochondrial transcription factor A is necessary for mtDNA maintenance and embryogenesis in mice. *Nat Genet*, **18**, 231-236.
20. Farge, G., Mehmedovic, M., Baclayon, M., van den Wildenberg, S.M., Roos, W.H., Gustafsson, C.M., Wuite, G.J. and Falkenberg, M. (2014) In vitro-reconstituted nucleoids can block mitochondrial DNA replication and transcription. *Cell Rep*, **8**, 66-74.
21. Lu, B., Lee, J., Nie, X., Li, M., Morozov, Y.I., Venkatesh, S., Bogenhagen, D.F., Temiakov, D. and Suzuki, C.K. (2013) Phosphorylation of human TFAM in mitochondria impairs DNA binding and promotes degradation by the AAA+ Lon protease. *Mol Cell*, **49**, 121-132.
22. Alam, T.I., Kanki, T., Muta, T., Ukaji, K., Abe, Y., Nakayama, H., Takio, K., Hamasaki, N. and Kang, D. (2003) Human mitochondrial DNA is packaged with TFAM. *Nucleic Acids Res*, **31**, 1640-1645.
23. Peter, B., Waddington, C.L., Olahova, M., Sommerville, E.W., Hopton, S., Pyle, A., Champion, M., Ohlson, M., Siibak, T., Chrzanowska-Lightowlers, Z.M.A. *et al.* (2018) Defective mitochondrial protease LonP1 can cause classical mitochondrial disease. *Hum Mol Genet*, **27**, 1743-1753.
24. Nagashima, S., Tabara, L.C., Tilokani, L., Paupe, V., Anand, H., Pogson, J.H., Zunino, R., McBride, H.M. and Prudent, J. (2020) Golgi-derived PI(4)P-containing vesicles drive late steps of mitochondrial division. *Science*, **367**, 1366-1371.
25. Bugiani, M., Invernizzi, F., Alberio, S., Briem, E., Lamantea, E., Carrara, F., Moroni, I., Farina, L., Spada, M., Donati, M.A. *et al.* (2004) Clinical and molecular findings in children with complex I deficiency. *Biochim Biophys Acta*, **1659**, 136-147.
26. Fernandez-Vizarra, E., Lopez-Perez, M.J. and Enriquez, J.A. (2002) Isolation of biogenetically competent mitochondria from mammalian tissues and cultured cells. *Methods*, **26**, 292-297.
27. Calvaruso, M.A., Smeitink, J. and Nijtmans, L. (2008) Electrophoresis techniques to investigate defects in oxidative phosphorylation. *Methods*, **46**, 281-287.
28. Sciacco, M. and Bonilla, E. (1996) Cytochemistry and immunocytochemistry of mitochondria in tissue sections. *Methods Enzymol*, **264**, 509-521.
29. Reyes, A., Kazak, L., Wood, S.R., Yasukawa, T., Jacobs, H.T. and Holt, I.J. (2013) Mitochondrial DNA replication proceeds via a 'bootlace' mechanism involving the incorporation of processed transcripts. *Nucleic Acids Res*, **41**, 5837-5850.
30. Farge, G., Pham, X.H., Holmlund, T., Khorostov, I. and Falkenberg, M. (2007) The accessory subunit B of DNA polymerase gamma is required for mitochondrial replisome function. *Nucleic Acids Res*, **35**, 902-911.
31. Al-Behadili, A., Uhler, J.P., Berglund, A.K., Peter, B., Doimo, M., Reyes, A., Wanrooij, S., Zeviani, M. and Falkenberg, M. (2018) A two-nuclease pathway involving RNase H1 is required for primer removal at human mitochondrial OriL. *Nucleic Acids Res*, **46**, 9471-9483.
32. Matulis, D., Kranz, J.K., Salemme, F.R. and Todd, M.J. (2005) Thermodynamic stability of carbonic anhydrase: measurements of binding affinity and stoichiometry using ThermoFluor. *Biochemistry*, **44**, 5258-5266.

33. Saneto, R.P., Lee, I.C., Koenig, M.K., Bao, X., Weng, S.W., Naviaux, R.K. and Wong, L.J. (2010) POLG DNA testing as an emerging standard of care before instituting valproic acid therapy for pediatric seizure disorders. *Seizure*, **19**, 140-146.
34. Stewart, J.D., Horvath, R., Baruffini, E., Ferrero, I., Bulst, S., Watkins, P.B., Fontana, R.J., Day, C.P. and Chinnery, P.F. (2010) Polymerase gamma gene POLG determines the risk of sodium valproate-induced liver toxicity. *Hepatology*, **52**, 1791-1796.
35. Bogenhagen, D. and Clayton, D.A. (1978) Mechanism of mitochondrial DNA replication in mouse L-cells: kinetics of synthesis and turnover of the initiation sequence. *J Mol Biol*, **119**, 49-68.
36. Doda, J.N., Wright, C.T. and Clayton, D.A. (1981) Elongation of displacement-loop strands in human and mouse mitochondrial DNA is arrested near specific template sequences. *Proc Natl Acad Sci U S A*, **78**, 6116-6120.
37. Nicholls, T.J. and Minczuk, M. (2014) In D-loop: 40 years of mitochondrial 7S DNA. *Exp Gerontol*, **56**, 175-181.
38. Do, Y., Matsuda, S., Inatomi, T., Nakada, K., Yasukawa, T. and Kang, D. (2020) The accessory subunit of human DNA polymerase gamma is required for mitochondrial DNA maintenance and is able to stabilize the catalytic subunit. *Mitochondrion*, **53**, 133-139.
39. Lee, Y.S., Kennedy, W.D. and Yin, Y.W. (2009) Structural insight into processive human mitochondrial DNA synthesis and disease-related polymerase mutations. *Cell*, **139**, 312-324.
40. Bezawork-Geleta, A., Brodie, E.J., Dougan, D.A. and Truscott, K.N. (2015) LON is the master protease that protects against protein aggregation in human mitochondria through direct degradation of misfolded proteins. *Sci Rep*, **5**, 17397.
41. Kereiche, S., Kovacik, L., Bednar, J., Pevala, V., Kunova, N., Ondrovicova, G., Bauer, J., Ambro, L., Bellova, J., Kutejova, E. *et al.* (2016) The N-terminal domain plays a crucial role in the structure of a full-length human mitochondrial Lon protease. *Sci Rep*, **6**, 33631.
42. Matsushima, Y., Goto, Y. and Kaguni, L.S. (2010) Mitochondrial Lon protease regulates mitochondrial DNA copy number and transcription by selective degradation of mitochondrial transcription factor A (TFAM). *Proc Natl Acad Sci U S A*, **107**, 18410-18415.
43. Macao, B., Uhler, J.P., Siibak, T., Zhu, X., Shi, Y., Sheng, W., Olsson, M., Stewart, J.B., Gustafsson, C.M. and Falkenberg, M. (2015) The exonuclease activity of DNA polymerase gamma is required for ligation during mitochondrial DNA replication. *Nat Commun*, **6**, 7303.
44. Di Re, M., Sembongi, H., He, J., Reyes, A., Yasukawa, T., Martinsson, P., Bailey, L.J., Goffart, S., Boyd-Kirkup, J.D., Wong, T.S. *et al.* (2009) The accessory subunit of mitochondrial DNA polymerase gamma determines the DNA content of mitochondrial nucleoids in human cultured cells. *Nucleic Acids Res*, **37**, 5701-5713.
45. Ruhanen, H., Borrie, S., Szabadkai, G., Tyynismaa, H., Jones, A.W., Kang, D., Taanman, J.W. and Yasukawa, T. (2010) Mitochondrial single-stranded DNA binding protein is required for maintenance of mitochondrial DNA and 7S DNA but is not required for mitochondrial nucleoid organisation. *Biochim Biophys Acta*, **1803**, 931-939.
46. Milenkovic, D., Matic, S., Kuhl, I., Ruzzenente, B., Freyer, C., Jemt, E., Park, C.B., Falkenberg, M. and Larsson, N.G. (2013) TWINKLE is an essential mitochondrial helicase required for synthesis of nascent D-loop strands and complete mtDNA replication. *Hum Mol Genet*, **22**, 1983-1993.
47. Stewart, J.D., Schoeler, S., Sitarz, K.S., Horvath, R., Hallmann, K., Pyle, A., Yu-Wai-Man, P., Taylor, R.W., Samuels, D.C., Kunz, W.S. *et al.* (2011) POLG mutations cause decreased mitochondrial DNA repopulation rates following induced depletion in human fibroblasts. *Biochim Biophys Acta*, **1812**, 321-325.
48. Khiati, S., Baechler, S.A., Factor, V.M., Zhang, H., Huang, S.Y., Dalla Rosa, I., Sourbier, C., Neckers, L., Thorgeirsson, S.S. and Pommier, Y. (2015) Lack of mitochondrial topoisomerase I (TOP1mt) impairs liver regeneration. *Proc Natl Acad Sci U S A*, **112**, 11282-11287.

49. Lee, Y.G., Kim, H.W., Nam, Y., Shin, K.J., Lee, Y.J., Park, D.H., Rhee, H.W., Seo, J.K. and Chae, Y.C. (2021) LONP1 and ClpP cooperatively regulate mitochondrial proteostasis for cancer cell survival. *Oncogenesis*, **10**, 18.
50. Zurita Rendon, O. and Shoubridge, E.A. (2018) LONP1 Is Required for Maturation of a Subset of Mitochondrial Proteins, and Its Loss Elicits an Integrated Stress Response. *Mol Cell Biol*, **38**.
7/4/2020 1:56:00 AM

Figure 1

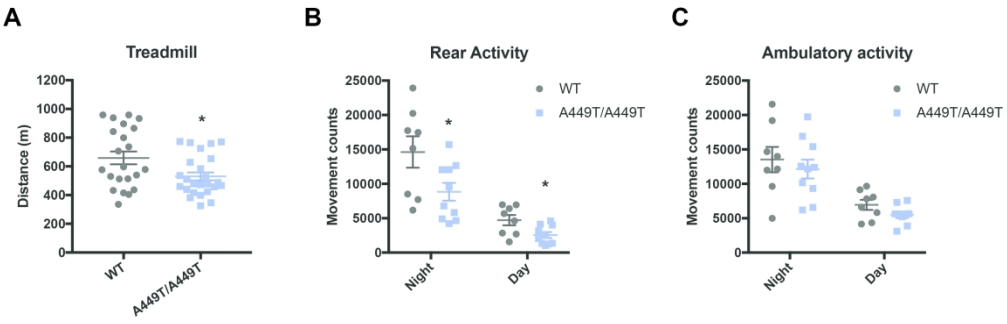

Figure 1. Characterization of the clinical phenotype of Polg$^{A449T/A449T}$ mice.

Figure 2

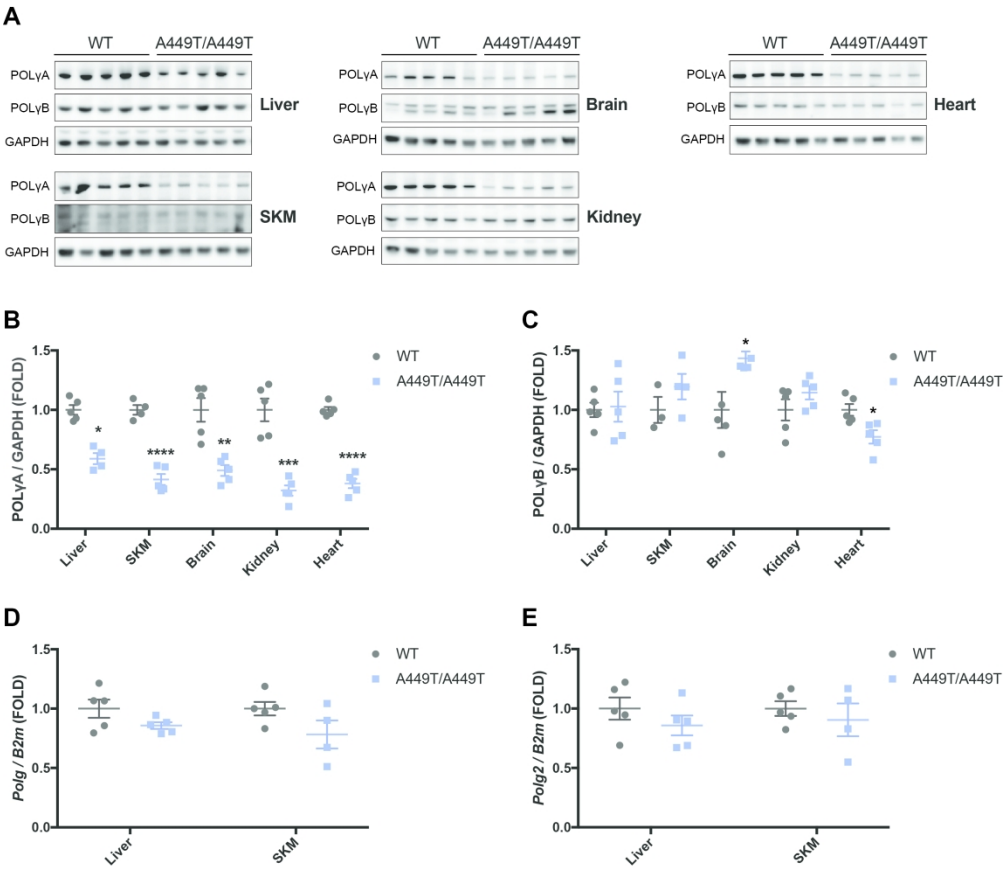

Figure 2. Characterization of PolγA and PolγB levels in tissues of Polg$^{A449T/A449T}$ mice.

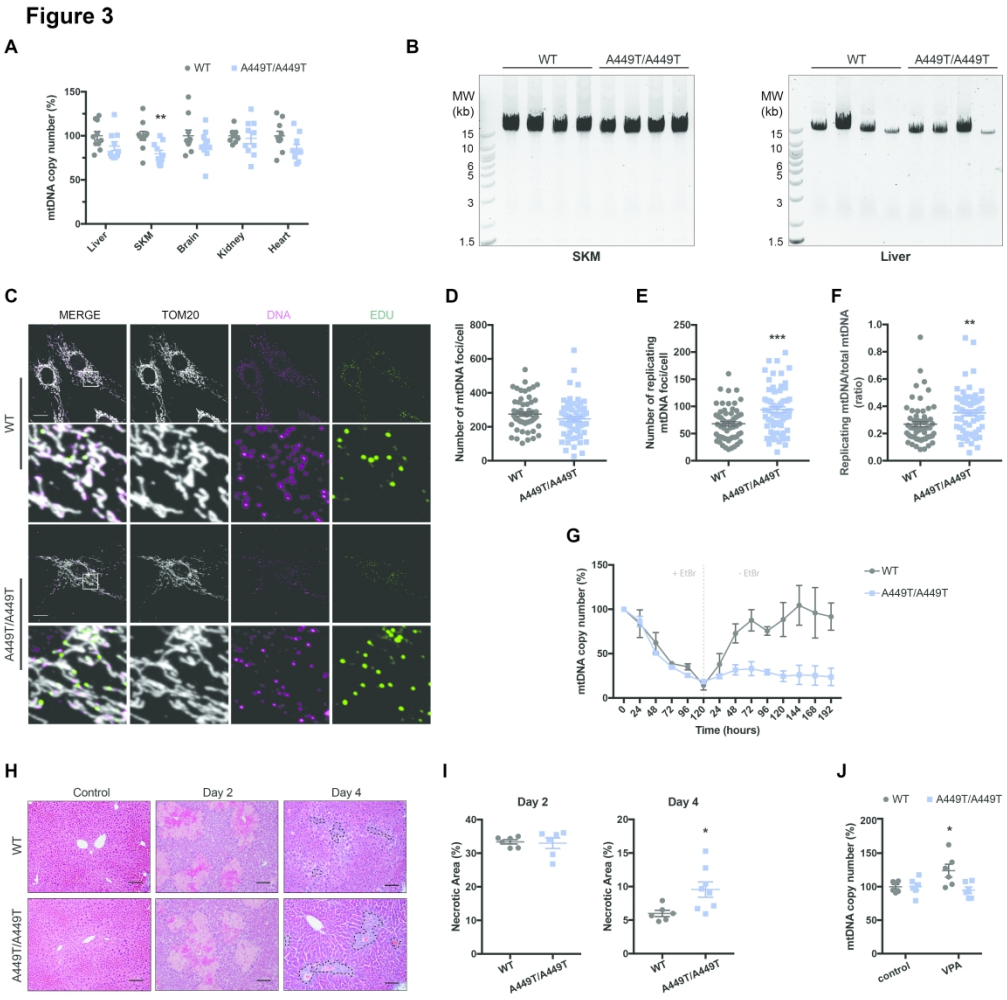

Figure 3. Characterization of the molecular phenotype of Polg$^{A449T/A449T}$ mice

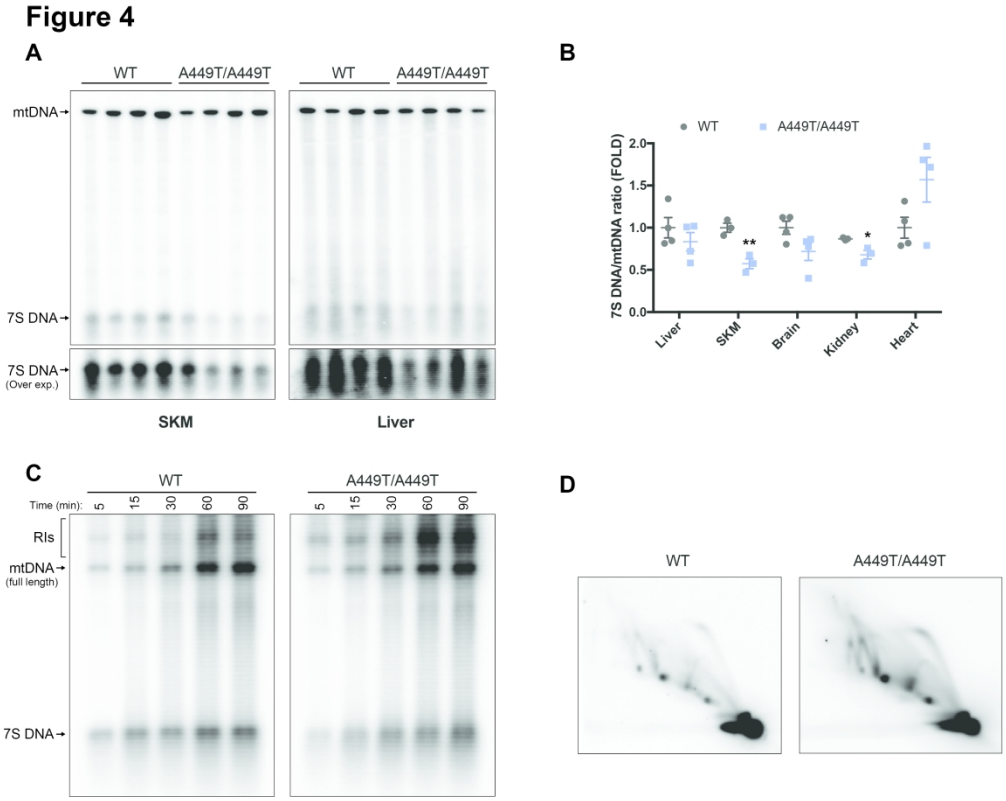

Figure 4. Molecular analysis of mtDNA replication in Polg$^{A449T/A449T}$ mitochondria

Figure 5

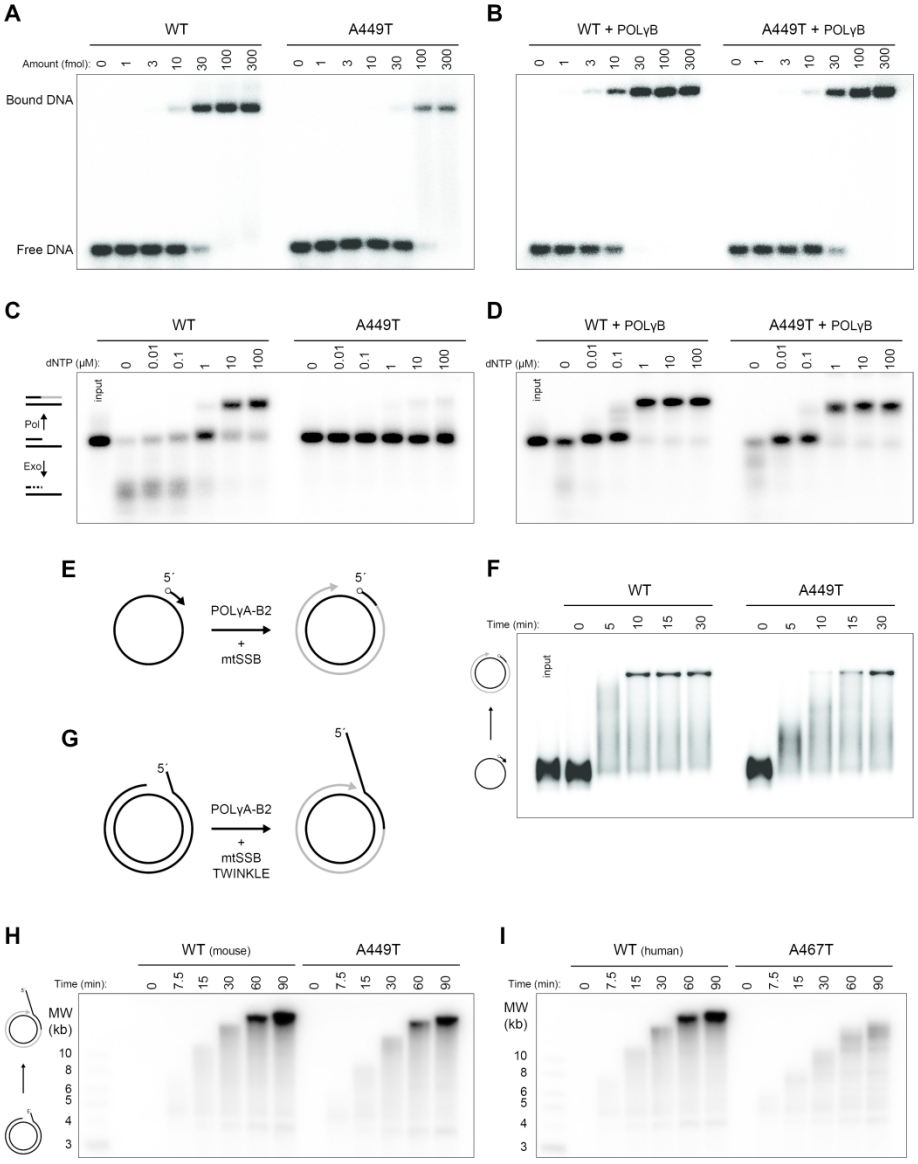

Figure 5. In vitro characterization of POLγA^{A449T} mutant protein

Figure 6

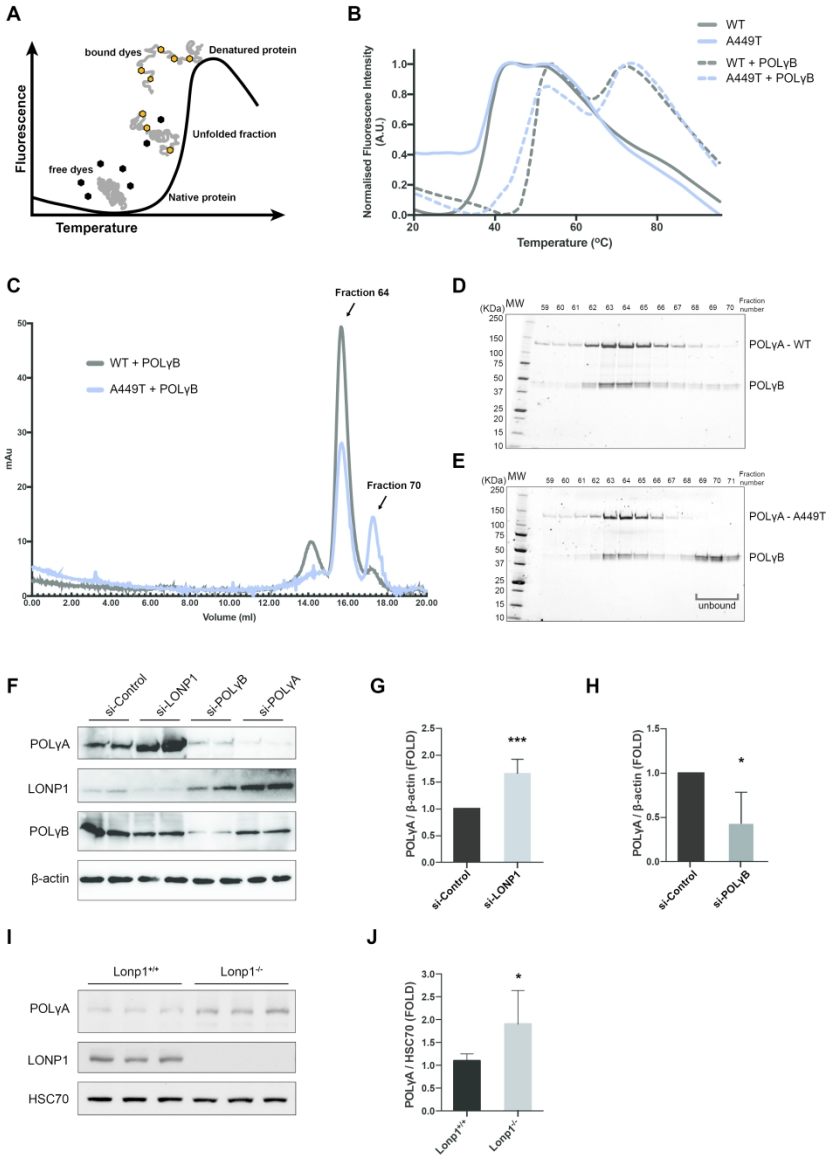

Figure 6. Stability of PolγA^{A449T} mutant protein in vitro and in vivo.

Figure 7

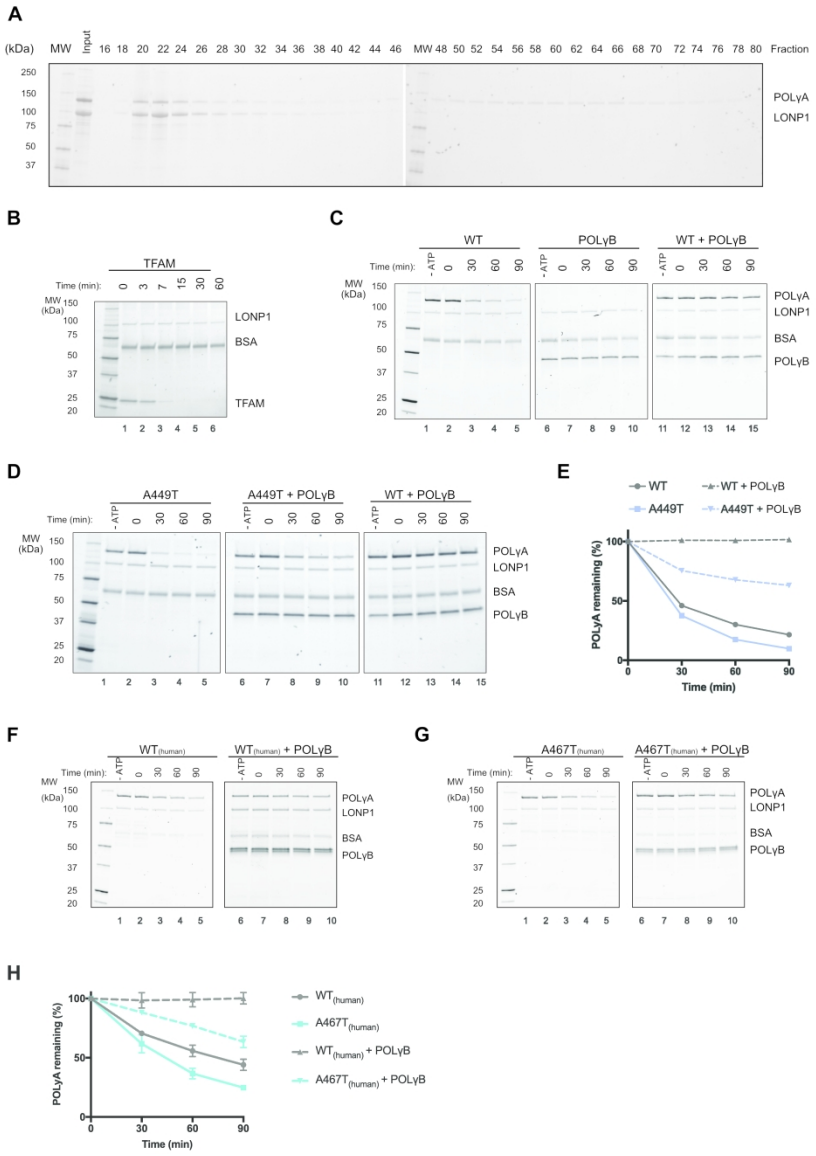

Figure 7. POLγA is a target of LONP1 degradation in vitro